This is to certify that the

dissertation entitled

ELECTRICAL TRANSPORT MEASUREMENTS BELOW 1K
ON COLD WORKED POTASSIUM

presented by

Shi Yin

has been accepted towards fulfillment
of the requirements for

Ph.D. degree in Physics

Major professor

Date 7/27/87

ELECTRICAL TRANSPORT MEASUREMENTS BELOW 1K ON COLD WORKED POTASSIUM

By

Shi Yin

A DISSERTATION

Submitted to
Michigan State University
in partial fullfillment of the requirements
for the degree of

DOCTOR OF PHILOSOPHY

Department of Physics and Astronomy

1987

ABSTRACT

ELECTRICAL TRANSPORT MEASUREMENTS BELOW 1K
ON COLD WORKED POTASSIUM

By

Shi Yin

The electron-dislocation interaction has been studied with an emphasis on resistivity for temperatures below 1K. Dislocations are introduced into the sample by twisting using a device driven by pressurized helium gas, and measurements of the temperature derivative of the resistivity, $d\rho/dT$, are made down to 20mK. 2mm-diameter samples are used to avoid the complication due to a size effect when the sample diameter is of the order of the electron mean free path. For deformed K(Rb) samples or deformed K samples with vacancies, a vibrating dislocation mechanism is observed; for deformed K samples in which the vacancies are annealed out at 60K, a new behavior in $d\rho/dT$ is observed which can be fit by a localized electronic-energy-level model together

with a residual contribution from the vibrating dislocations. A possible Charge Density Wave contribution is also discussed. A comparison with previous experimental work is made. Thermoelectric ratio measurements are also reported and discussed.

TO MY WIFE

ACKNOWLEDGMENTS

I wish to thank Professor William P. Pratt Jr. for his supervision and invaluable aid in all aspects of this dissertation. I am particularly grateful for the many late nights worked while taking data.

I extend a thanks to Professor Peter A. Schroeder for many late nights worked together and many helpful advices.

I also extend a thanks to Mr. Fred Freiheit for his help in designing the sample can.

I acknowledge the finacial support of the National Science Foundation and Michigan State University.

TABLE OF CONTENTS

Page

LIST OF TABLES - viii

LIST OF FIGURES - ix

INTRODUCTION - 1

Chapter

I Basic Electrical Transport Theory - - - - - - - - - - - - - - - - 3

1.1 Resistivity - 3

1.1.1 The residual resistivity due to dislocations - - - - 5

1.1.2 Electron-phonon scattering - - - - - - - - - - - - - - - 11

1.1.3 Electron-electron scattering - - - - - - - - - - - - - - 16

1.1.4 Electron-dislocation scattering - - - - - - - - - - - - 19

1.1.5 Electron-phason scattering and Charge Density Waves (CDW) - 23

1.2 Thermoelectric power - 26

1.2.1 Diffusion thermopower - - - - - - - - - - - - - - - - - 26

1.2.2 Phonon drag thermopower - - - - - - - - - - - - - - - - 28

1.2.3 Thermoelectric ratio - - - - - - - - - - - - - - - - - - 29

II Experimental Techniques - 32

2.1 Main equipment for measurements - - - - - - - - - - - - - - - 32

2.1.1 The dilution refrigerator - - - - - - - - - - - - - - - 32

2.1.2 The high precision resistance bridge - - - - - - - - - 33

2.1.3 The screened room and floating pad - - - - - - - - - - 33

2.1.4 A schematic diagram of the ultralow temperature part of the cryostat - - - - - - - - - - - - - - - - - - -33

2.2 The thermometry -35

2.3 Sample can - 40

2.4 Plastic deformation of the sample - - - - - - - - - - - - - -45

2.5 Sample preparation - 48

2.6 Measurements - 53

2.7 Heat loss -60

2.8 Heat generated while deforming the sample - - - - - - - - -63

2.9 Uncertainties -65

III Experimental Results -67

3.1 Resistivity -67

3.1.1 Residual resistivity - - - - - - - - - - - - - - - - - - 67

3.1.2 K(Rb) data - 70

3.1.3 Pure K data without annealing - - - - - - - - - - - - - 75

3.1.4 Pure K data after annealing - - - - - - - - - - - - - -84

3.1.5 Annealing at 60K after deforming at 9.3K vs deforming directly at 60K for pure K samples - - - - 92

3.1.6 Comparison of 60K annealed pure K sample with those of Harele *et al.* - - - - - - - -92

3.2 Thermoelectric Ratio - 95

IV Discussion and Conclusions - - - - - - - - - - - - - - - - - -103

LIST OF REFERENCES - 109

LIST OF TABLES

Table		Page
2.1	A list of parts in sample can	42
2.2	Chemical analysis of potassium	51
3.1	K (0.087 at% Rb) alloy sample	72
3.2	Pure K sample without annealing	79
3.3	Pure K sample with A as a variable parameter	88
3.4	Pure K samples after annealing or deformation at 60K	90
3.5	Parameters in G for the K(Rb) and K samples	98

LIST OF FIGURES

Figures		Page
1.1	An edge dislocation (a) and a screw dislocation (b)- - - -	-6
1.2	Screw dislocations Two neighbouring planes in a simple cubic lattice rotated slightly with respect to each other. A regular pattern of screw dislocations is visible. The (001) direction is perpendicular to the page - - - - - - - - - - - - - - - -	7
1.3	The phonon processes -	-12
2.1	The low temperature part of the cryostat - - - - - - - - - -	-34
2.2	The CMN thermometer -	37
2.3	Circuits of the CMN mutual inductance bridges - - - - - - -	39
2.4	Sample can -	-41
2.5	A perspective view of the sample holder - - - - - - - - - -	44
2.6	A perspective drawing of the twister mechanism - - - - - -	46
2.7	The He pressurization system for the bellows - - - - - - -	-49
2.8	The press and die for extruding the sample- - - - - - - -	-52
2.9	The low temperature circuit - - - - - - - - - - - - - - -	55
2.10	The Ag sample mount The Ag sample mount on which the thermometers etc. are mounted -	61
3.1	$\Delta\rho_e$ vs θ $\Delta\rho_e$ is plotted as a function of the angle of twist for sample K-5(open circle). The full circles are the data from van Vucht et al. -	-69
3.2	$d\rho/dT$ vs T for K(Rb) samples $d\rho/dT$ is plotted as a function of T for the K(Rb) samples in a series of twists. The details are given	

in Table 3.1 -71

3.3 $d\rho/dT - (2AT-C')$ vs T for K(Rb) samples
$d\rho/dT - (2AT-C')$ is plotted as a function of T for the K(Rb) samples. A step-like function is seen for samples KRb-4 and KRb-5 - 74

3.4 $(\rho_{4.2}/\rho)d\rho/dT$ vs T for pure K samples
The samples are twisted at 9.3K without annealing. The details of twist are given in Table 3.2. - - - - - - - - - - 77

3.5 $(\rho_{4.2}/\rho)d\rho/dT - 2A'T$ vs T for the unannealed K samples
A step-like function is seen. The solid and dashed curves are the best computer fits. Details are given in the text - 78

3.6 A two-frequency fit vs the one-frequencey for sample K-5
An improved fit is obtained - - - - - - - - - - - - - - - - - - 81

3.7 D vs $\Delta\rho_o$ the K(Rb) and K samples
The coefficient D of Eq.(3.3) or Eq.(3.6) is plotted as a function of $\Delta\rho_o$ for the K(Rb) samples or pure K samples without annealing. The data from Haerle et al. are also shown. The dashed line is the fit to the K samples after the vacancy contribution is corrected for, see text for details - - - - - - - - - - - - - - - - - -82

3.8 E vs $\Delta\rho_o$ for K(Rb) and K samples
The characteristic energy E is plotted as a function of $\Delta\rho_o$ for the K(Rb) and K samples. The data from Haerle et al. are in agreement with ours. - - - - - - - - - - - - - -85

3.9 $(\rho_{4.2}/\rho)d\rho/dT - 2A'T$ vs T for the annealed pure K samples
A peak is seen at 0.2K. The dashed curve is the best fit for the unannealed sample K-5. The solid curves are explained in the text - 87

3.10 The improved fit to K-7 with A as a variable parameter
The dashed curve is without the CT^5 term. A CT^5 term helps to fit the rising tail of the data.- - - - - - - - - - - - - -89

3.11 A comparison between annealing at 60K after twisting at 9.3K (K-7) and twisting directly at 60K (K2-2)
A similar behavior is seen. The data of Haerle et al. are also presented- 93

3.12 G vs T for the K(Rb) samples
Details of the fit are given in the text - - - - - - - - - -96

3.13 G vs T for the pure K samples - - - - - - - - - - - - - - - -97

3.14 The Gorter–Nordheim plot for both K(Rb) and K samples
$\mathcal{G}_d$ seems to be the same in both cases - - - - - - - - - - - - 100

3.15 b vs $\Delta\rho_o$ for both K(Rb) and K samples
A systematic change is visible- - - - - - - - - - - - - - - - - - 102

INTRODUCTION

Potassium has long been a material of considerable theoretical and experimental interest. Most people believe that potassium has the simplest electronic structure in comparison with non-alkali metals. It has a nearly spherical Fermi surface which is entirely contained with in the first Brillouin zone, and it has no unfilled d- or f- shells. Thus the nearly free electron model is a good approximation for many calculations, making transport theory comparatively easy to carry out. Furthermore, in contrast to potassium, lithium, sodium, and possibly even rubidium(1) undergo Martensitic phase transformations at low temperatures which complicate the interpretation of measurements. Potassium is also a good testing ground for the existence of Charge Density Waves (CDW), which are a broken translational symmetry of the ground state. Recently, two new experiments have addressed this CDW hypothesis: the observation of CDW satellites in potassium by Giebultowicz *et al.*(2) in their neutron diffraction experiment and the failure in detecting such satellites by H. You *et al.* (3) in their synchrotron X-ray diffraction experiment. If found to exist, CDW would radically change our basic understanding of transport in such a simple metal.

In this study we are going to report the effect of electron-dislocation interaction on the transport properties of potassium, where the dislocations are produced through deformation of

polycrystalline potassium samples. Since deformation of K might also change the Q-domain textures of CDW's in potassium (4), the effect of CDW's will also be discussed.

This study was begun by Mark L. Haerle et al.(5)(6), and the results reported here are a continuation of their work with three significant improvements: Firstly, we introduce the dislocations into our sample by twisting with a device driven by pressurized helium gas, while Haerle et al. did it by squashing the sample between two plates. In our method of deformation the sample geometry change $\Delta(A/L)$, where A is the sample cross sectional area and L is the sample length, is much better controlled (<1%) than that of Haerle's (<10%). Since the resistivity $\rho = R(A/L)$, any change in A/L during deformation would make it difficult to tell the real contribution of dislocations to ρ. Secondly, we have used a different dilution refrigerator which can obtain a much lower temperature (T>20 mK) than that of Haerle et al. (T>80 mK). This new region of temperature is crucial for determining the low-energy vibration spectrum associated with the dislocations. Finally, we used 2mm diameter samples to avoid a possible size effect which made the analysis of Haerle's 0.9mm diameter samples more complicated.

Chapter I Basic Electrical Transport Theory

The fundamental basis for electrical transport study is the following set of equations

$$J = L_{11}E + L_{12}\nabla T \tag{1.1}$$

$$\dot{Q} = L_{21}E + L_{22}\nabla T \tag{1.2}$$

where J is the electric current density, $\dot{Q}$ is the heat flow current density, E is the electric field, and ∇T is the temperature gradient. The L_{ij} coefficients are tensors in general, but they can be reduced to scalars here because potassium has cubic symmetry.

In this work we mainly measure the electrical resistivity ρ and the thermal power S. They are defined as follows

$$\rho^{-1} = \sigma = (J/E)\Big|_{\nabla T=0} = L_{11} \tag{1.3}$$

$$S = (E/\nabla T)\Big|_{J=0} = -L_{12}/L_{11} \tag{1.4}$$

1.1 Resistivity

Theory predicts that the resistivity for Bloch electrons in a perfect lattice is zero, and the finite resistance in a real metal comes from the interactions of the conduction electrons with the

imperfections of the lattice such as impurities, dislocations, lattice vibrations, etc. If Matthiessen's rule is obeyed, one can write down the resistivity of potassium as a sum of terms

$$\rho = \rho_o + \rho_{ep} + \rho_{ee} + \rho_{other} \qquad (1.5)$$

where ρ_o is the residual resistivity, which is independent of temperature and is due to scattering by various static imperfections in the crystal. The second term ρ_{ep} is usually a function of temperature: $\rho_{ep} = \rho_{ep}(T)$. It is due to electrons scattering off phonons. The third term ρ_{ee} is the electron-electron scattering term, and it is also temperature dependent: $\rho_{ee} = \rho_{ee}(T)$. This term is usually 10^4 times smaller than the residual resistivity ρ_o in pure potassium at 1K.

The last term can be expressed as a sum of terms for other possible contributions to ρ. The resistivity due to electrons scattering off phasons, $\rho_{e\text{-}ph}$ which are the elementary excitation of CDWs, is one of these possible terms. Because of the recent observation of CDW satellites in potassium by Giebultowicz *et al.*(2), a phason-scattering term in ρ can not be ruled out.

Another possible term is ρ_{ed}, which is the resistivity due to interactions between electrons and dislocations. Normally one would expect ρ_{ed} to be temperature independent and thus only contribute to ρ_o. However, the work of Haerle has shown that there is also a temperature dependent term which is of interest in this thesis. A dislocation is an extended line-defect in a crystal. There are basically two kinds of

dislocations: the edge dislocation and screw dislocation. For an edge dislocation the Burgers vector b is perpendicular to the dislocation line, and for a screw dislocation b is parallel to the dislocation line(Fig. 1.1).

In our experiment we introduce the dislocations into our sample by twisting. Ideally, torsional deformation along (001) direction in a cubic symmetry crystal will produce networks of equally spaced screw dislocations in two perpendicular directions (Fig. 1.2). However, for our polycrystalline samples the sample axis is not parallel to any particular symmetry direction, and there may be imperfections like vacancies or other dislocations already present in the sample before we deform it. We therefore expect to produce a very irregular dislocation structure during deformation. As we will see later, the temperature at which we deform the sample and the possible subsequent annealing will play an important role in affecting the detailed structure of these imperfections.

1.1.1 The residual resistivity due to dislocations

There are several theories that explain the origin of the residual resistivity. Of particular interest here are those which address electron scattering by dislocations.

Using a geometrical model of obstacles at which the conduction electron energy dissipates, Tsivinskii (7) calculated classically the residual resistivity due to impurities, vacancies and dislocations.

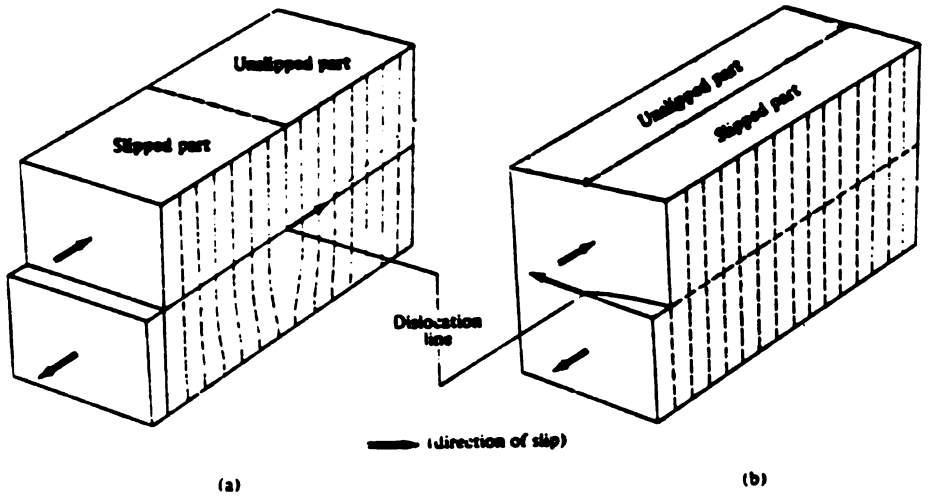

Figure 1.1
An edge dislocation (a) and a screw dislocation (b).

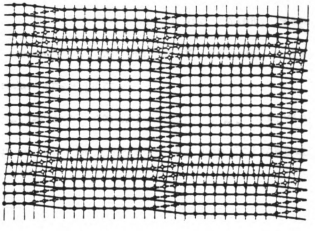

Figure 1.2
Screw dislocations
Two neighbouring planes in a simple cubic lattice rotated slightly with respect to each other. A regular pattern of screw dislocations is visible. The (001) direction is perpendicular to the page.

From this classical theory the resistivity is given by

$$\rho = (2mv/e^2n_e)(1/\lambda) \qquad (1.6)$$

where e and m are electron charge and mass, respectively, n_e is the free electron concentration per unit volume, v is the Fermi velocity, and λ is the mean free path.

For a dislocation contribution to ρ, Tsivinskii argued that the mean free path λ can be replaced by the following formula:

$$\lambda = 1/bN \qquad (1.7)$$

where N is the dislocation density(#/cm^2) and b is approximately equal to the magnitude of the Burgers vector. In this way, we obtain

$$\rho = 2mvbN/e^2n_e = WN \ . \qquad (1.8)$$

For potassium, Eq. (1.8) predicts that

$$W = 1.6\text{x}10^{-19} \ (\Omega\text{cm}^3). \qquad (1.9)$$

This value of W is almost a factor of 2 smaller than the experimental value obtained by Basinski et al. (8).

For the contribution of impurities or vacancies Tsivinskii uses

$$\lambda = 1/[\pi n(x^2-x_o^2)] \qquad (1.10)$$

in which n is the atomic concentration per unit volume of the metal, and x and x_o are ionic and impurity radii, respectively. For vacancies $x_o=0$.

Another theory was proposed by Basinski et al.(8) in which they calculated the mean atomic displacement from equilibrium due to the strain field around a dislocation. They asked what temperature is needed to give the same mean displacement via random thermal motion. Then they assumed that the increase in ρ due to the dislocation is the same as the resistivity due to the electron-phonon interaction at this temperature. They derived $W = 4\times10^{-19}\ \Omega cm^3$ in formula (1.8) for potassium, which is in good agreement with the experiment they performed.

In a third theory, Brown(9) calculated the resistivity due to resonant s-wave scattering of the electrons. The resonance is created by virtual bound states which are associated with the dislocation cores. He predicted that

$$\rho = WN_d \qquad (1.11)$$

where for potassium $W = 8\times10^{-19}\ \Omega cm^3$ which is a factor of 2 larger than the experimental value from Basinski(8) et al. Brown argued against a correction factor used by Basinski in obtaining their experiment result which, if omitted, would bring Brown's theory in closer agreement with

experiment.

Gurney and Gugan(10) performed an early study of the effects on the residual resistivity of annealing a wire of deformed potassium. In their experiment the residual resistivity was measured first, and then the sample was plastically deformed at 4.2K. Again ρ_o was measured. Next the sample was annealed at a higher temperature and then slowly cooled down to 4.2K where ρ_o was measured. They kept annealing and measuring ρ_o in stages until the initial value of ρ_o was recovered. The Gurney and Gugan interpretations, which are significant to this thesis, are as follows:

1. Between 3 and 7K, the relatively few interstitials formed during deformation anneal out, causing about 5% resistivity decrease.

2. Between 10 and 20K, about 40% of the extra resistivity caused by deformation disappears. This is ascribed to the long-range migration of monovacancies. There is evidence that the dominant processes at the end of this stage involve the annihilation of defects at dislocation sinks.

3. Between 20 and 80K, there is a region with no significant peaks in the recovery rate, but over this temperature range about 30% of the deformation-produced resistivity disappears. Part of this is attributed to the detrapping of point defects, probably vacancies, from impurities.

4. Between 80 and 150K, the recovery rate shows a strong peak at about 110K and accounts for 25% of the total recovery. This is associated with the annealing of dislocations during recrystallization.

5. Between 5 and 20K, a major length recovery occurs considerably before the resistivity recovery begins. Gugan(11) ascribes this to a rearrangement of dislocations rather than a decline in the number of dislocations.

These temperature ranges are rough guesses based on the breaking points in the complicated annealing curves of residual resistivity vs the annealing temperature, and some of the proposed mechanisms which explain the various recovery stages are unsubstantiated. Nonetheless, this study does provide a basis on which the effects of dislocations on the resistivity may be examined.

1.1.2 Electron-phonon scattering

In calculating the electron-phonon interaction, the following condition must be satisfied in order to obtain a non-vanishing matrix element:

$$\vec{K}' - \vec{K} = \pm \vec{q} + \vec{G} \qquad (1.12)$$

where $\vec{K}$ and $\vec{K}'$ are the wave vectors for the incoming and scattered electrons, respectively, $\vec{q}$ is the phonon wave vector, and $\vec{G}$ is the reciprocal lattice vector. The plus or minus sign before q represents the phonon absorption or emission processes. If $\vec{G}\neq 0$, the process is called Umklapp; and if $\vec{G}=0$, it is the normal process.

The above phonon processes are illustrated in Fig. 1.3, where

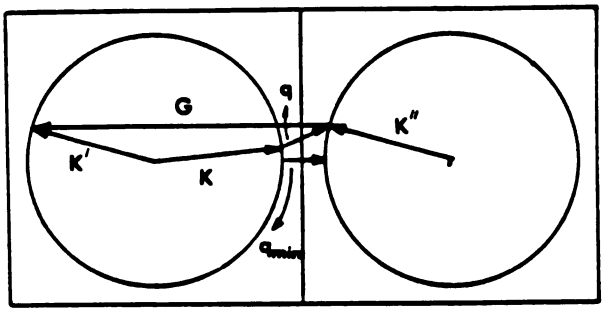

1) Umklapp process

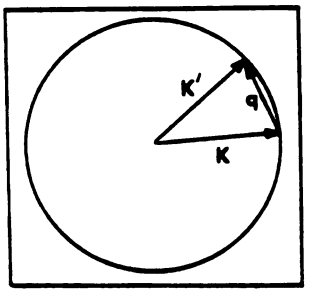

2) normal process

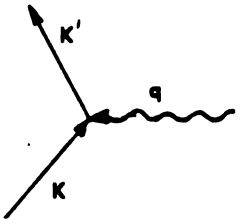

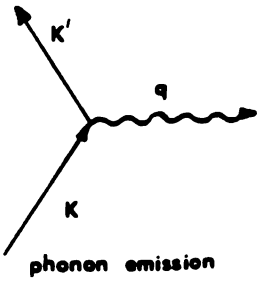

3) phonon absorption phonon emission

Figure 1.3
The phonon processes

potassium is assumed to have a nearly spherical Fermi surface which does not touch the first Brillouin zone. This figure illustrates

1) The Umklapp process. When the magnitude of the emitted or absorbed phonon wave vector q exceeds the minimum value — q_{min}, this process can occur. The characteristic feature of this process is that even when the value of q is small there can be a large difference between the directions of $\vec{K}$ and $\vec{K}'$.

2) The normal process. The crystal momentum is conserved here.

3) The phonon absorption or emission.

By assuming an equilibrium phonon distribution, a relaxation time approximation for the Boltzmann equation, no Umklapp scattering, and a Debye spectrum for phonons, Bloch(12) predicted that the electrical resistivity due to electron-phonon scattering has the following temperature dependences for the indicated limits:

$$\rho(T) \propto T \quad , \tag{1.13}$$

for $T > 0.5\theta_D$, and

$$\rho(T) \propto T^5 \quad , \tag{1.14}$$

for $T < 0.1\ \theta_D$, where θ_D is the Debye temperature.

Since θ_D for potassium is about 100K, we therefore expect to have in our experiment below 1K

$$\rho_{ep} = CT^5, \qquad (1.15)$$

where C is a constant. However, measurements done by Gugan(13) (T>1.2K), Ekin and Maxfield(14) (T>1.5K) and van Kempen et al.(15) (T>1.1K) did not show this T^5 term. Instead their results could be fit to an equation of the form

$$\rho_{ep}(T) = BT^n EXP(-\theta'/T) \qquad (1.16)$$

with $n \sim 1$ and $\theta' \sim 20K$. When T is less than or equal to 1K, this exponential term is negligible; and the data from Haerle et al.(6) (T<1K) also failed to show the T^5 behavior in their unstrained potassium samples.

The main reason for the failure of this model is attributed to the presence of phonon drag (13). Basically phonon drag arises when the phonon distribution is disturbed from its equilibrium state at low temperatures. According to Danino, Kaveh and Wiser(16), the electrical resistivity is caused by the electron system transfering its excess momentum, gained from the electric field, to the phonon system via electron-phonon scattering. However, at low temperatures, much of this excess momentum is not dissipated by the phonons (not lost to the lattice), but is returned to the electron system via phonon-electron scattering. The electrons are thereby "dragged" along by the phonons (phonon drag), so that there are less effective electron-phonon scatterings, and therefore the electrons experience a much reduced

resistivity. In potassium at low temperatures, such a phonon drag process can largely eliminate the normal scattering contribution (CT^5) to the resistivity(17); and at high temperatures this effect is quenched because phonon-phonon Umklapp scattering equilibrates the phonons with the lattice.

The exponential behaviour seen experimentally in $\rho_{ep}(T)$ can be understood in terms of electron-phonon Umklapp scattering, which is the scattering between two Brillouin zones. For potassium, this scattering requires phonons with at least the minimum momentum (q_m) to jump the gap between the two cells. Phonons obey Bose-Einstein statistics, and at low temperatures the density of phonons which can participate in an Umklapp process goes like

$$\exp(-\hbar v q_m/kT) \qquad (1.17)$$

where v is the velocity of the phonons. This factor dominates the electron-phonon resistivity seen experimentally; and at temperatures below 1K, which is the temperature range of present interest, this term is negligible.

There are mechanisms other than phonon-phonon Umklapp scattering that can pull the phonons into equilibrium. For example, a high concentration of impurities or dislocations(18) could interact with the phonons to provide a way for the phonons to lose the momentum given to them by the electrons, resulting in an equilibrium distribution.

Danino, Kaveh and Wiser(19) pointed out that the quenching of

phonon drag by phonon-dislocation scattering is likely to be negligible for potassium above 2K unless $N_d > 10^{10}$ cm^{-2}, where N_d is the dislocation density. For dislocation density $N_d \sim 10^9$ cm^{-2}, they and independently Engquist(20) proposed a new electron-dislocation interaction mechanism, which is based on the anisotropy of electron-dislocation scattering, to explain the suppression of phonon drag in the electrical resistivity of potassium.

1.1.3 Electron-electron scattering

Electron-electron scattering can contribute to the resistivity. Let $\vec{K}_1$ and $\vec{K}_2$ be the initial wave vectors of the two scattering electrons, and let $\vec{K}_3$ and $\vec{K}_4$ be the final wave vectors. Then we have the following momentum conservation rule

$$\vec{K}_1 + \vec{K}_2 = \vec{K}_3 + \vec{K}_4 + \vec{G} \qquad (1.18)$$

If $\vec{G}=0$, we have a normal process, and otherwise we have an Umklapp process.

In a calculation of the resistivity, we know from Ziman(21) that an approximate solution to the Boltzman equation for a normal e-e scattering process contains a factor of the following form:

$$[(\tau(\vec{K}_1)\vec{K}_1 + \tau(\vec{K}_2)\vec{K}_2 - \tau(\vec{K}_3)\vec{K}_3 - \tau(\vec{K}_4)\vec{K}_4)\cdot\hat{U}]^2 \cdot \delta(\vec{K}_1 + \vec{K}_2 - \vec{K}_3 - \vec{K}_4) \qquad (1.19)$$

where $\tau(K)$ is the electron relaxation time, and U is a unit vector in the direction of the electric field. When the scattering is isotropic, τ is a constant, and this term vanishes. Thus the normal process will not contribute to the resistivity. In the second order approximation the Umklapp process can take place, and the delta function given above is replaced by

$$\delta(\vec{K}_1+\vec{K}_2-\vec{K}_3-\vec{K}_4-\vec{G}) \ . \qquad (1.20)$$

So we see that Umklapp scattering gives a finite contribution to resistivity even with the isotropic relaxation time approximation. The calculation predicts a T^2 dependence of the e-e scattering contribution to the resistivity for $T \ll E_F/k_B$.

This T^2 behaviour has been observed experimentally by van Kempen et al.(22) and Levy et al.(23). However, some controversy arose when Rowlands et al.(24), who were the first to carry out high precision measurements below 1.2K, found that the resistivity of their potassium sample(0.79 mm in diameter) behaved more like $T^{1.5}$ than like T^2. Overhauser(25) tried to explain this $T^{1.5}$ behaviour on a CDW basis. Later Lee et al.(26) measured $\rho(T)$ for a number of thicker samples and confirmed the existence of a T^2 term down to 0.4K. Then Yu et al.(27) measured a series of samples with diameters ranging from 0.09 to 1.5 mm and found important deviations from T^2 behaviour in samples thinner than 1mm. Their interpretation invokes an effect proposed by Gurzhi(28) involving interference between normal electron-electron scattering and

surface scattering. Since Haerle et al.(5) used 0.9mm diameter samples in their deformation experiment, this size effect was present. Our experiment is better because we used 2mm diameter samples where the size effect is negligible.

As for the coefficient A of this T^2 term, a theory was worked out for potassium by Lawrence and Wilkins(29) for a screened Coulomb interaction. This theory was later refined by MacDonald et al.(30), who included both screened Coulomb scattering and phonon exchange scattering. MacDonald et al. found that the screened Coulomb interaction gave a much smaller contribution than the earlier work of Lawrence and Wilkins, and instead they found that the dominant term was due to phonon exchange scattering. Both theories predicted an AT^2 term with $A = 1.7\ f\Omega m/K^2$.

However, this coefficient A has been found by various groups mentioned above to be sample dependent, which conflicts with the fundamental ideas underlying the calculations of A. A way had to be found to introduce a non-intrinsic property, varying from sample to sample, which affected the magnitude of A. As we mentioned earlier, the normal electron-electron scattering does not contribute to the resistivity if the relaxation time τ is isotropic, as shown in Eq. (1.19). However, if τ is not isotropic, this term will not vanish and therefore can make a significant contribution to ρ. Kaveh and Wiser (31) argued that dislocations are the best candidate for such an anisotropic scatterer. At very low temperatures the dominant mechanisms are impurity(ρ_{ei}) and dislocation(ρ_{ed}) scatterings, and impurity

scattering is believed to be almost isotropic. Thus the ratio ρ_{od}/ρ_{oi} is a measure of the relative amount of anisotropic scattering, where

$$\rho_o = \rho_{oi} + \rho_{od}. \qquad (1.21)$$

Kaveh and Wiser obtained

$$A = A_0 + A_1 \rho_{od}^2/(\rho_{oi} + \rho_{od})^2 \qquad (1.22)$$

where A_0 is the Umklapp contribution in the isotropic limit, and A_1 corresponds to the maximum contribution from normal scattering. An estimate of A_1 is difficult because the anisotropy of the electron-dislocation scattering time is not known. Kaveh and Wiser estimated this anisotropy and were able to fit Eq.(1.22) to the data, although somewhat arbitrary estimates of ρ_{od}/ρ_{oi} were made for each set of data. They found that $A_1 = 3.5\ f\Omega m/K^2$ and $A_0 = 0.5\ f\Omega m/K^2$. The squashing experiments of Haerle et al.(6) were designed to test this theory by introducing a known value for ρ_{od}. Haerle et al. observed that $\rho(T)$ for deformed potassium did not exhibit the predicted T^2 behavior, which is in agreement with the results to be presented here. Thus the theory of Kaveh and Wiser, although important for motivating these deformation experiments, cannot explain these results, and different electron-dislocation scattering mechanisms are needed.

1.1.4 Electron-dislocation scattering

In his attempt to explain the residual resistivity due to dislocations, Brown(9) proposed a theory where the electrons are scattered primarily by the dislocation cores rather than by the surrounding strain fields. As a result, the large angle scattering by a segment of a dislocation line is independent of the proximity of other dislocations. He also stated that there is no reason to distinguish between the cores of edge, screw, or mixed character dislocations in this regard. He suggested that dislocations could have virtual bound states for electrons, with an energy slightly above the Fermi surface. He estimated that these relative energy levels for potassium are about 10^{-4}eV. These energy levels could be localized near the cores of the dislocations. Recently, Fockel(32) pointed out that the potential of the dislocation core contains resonance states below the Fermi energy. Fockel used the pseudo-potential concept in which he treated the core as discrete and the surrounding matrix as a non-linear elastic continuum.

Let us suppose that there are some localized electronic levels near the dislocation cores at some height E above (or below) the Fermi level and that they become occupied (or unoccupied) as temperature rises. Therefore the effective core charge changes with temperature. Gantmakher and Kulesco(33) derived the following equation assuming that the electrons were scattered elastically off the localized levels:

$$\rho_{ed}(T) = a(1+b\exp(E/k_BT))^{-1} \qquad (1.23)$$

where b is the spin degeneracy of the level and a is a proportionality constant.

There are other calculations which apply to interactions with localized energy levels in crystals. Fulde and Peschel(34) calculated the resistivity due to electrons scattering inelastically off localized energy levels produced by a crystalline electric field splitting of rare earth ions dissolved in metals. By using Matthiessen's rule, they derived the following expression

$$\rho(T) = \rho_0 \left[1 + \frac{G^2}{1 + (2/3)\sinh^2\left(\frac{D}{2T}\right)} \right] \qquad (1.24)$$

where G and ρ_0 are constants, and D is the energy level splitting for an assumed doublet. Even though this expression is not directly associated with dislocations, we think this theory might be applicable to scattering from local electron states caused by dislocations such as the virtual bound states predicted by Brown.

O'Hara and Anderson(35)(36), in their study of the lattice thermal conductivity on some superconducting metals, found the existence of a resonant phonon-dislocation interaction at certain frequencies. This work supports the existence of dynamic dislocations at low temperatures. They proposed two models for the possible vibrating dislocations. One was originated by Granato(37) in which the dislocation is treated as an elastic band stretched between two pinning points a distance L apart and the natural resonant frequency ν is given

by

$$\nu = V/3L \qquad (1.25)$$

where V is the transverse phonon velocity and L is the dislocation length. Hence the frequency is inversely proportional to L. The pinning source might be the intersection of a dislocation with other dislocation lines, vacancies or impurities. The other model is associated with the Peierls potential, which is important for bcc metals such as potassium for a reason we are going to discuss below. Here the dislocation might oscillate in its potential well with a frequency essentially independent of the length of the segment involved(35):

$$\nu = [\tau_p/4\pi^2\rho_m b^2]^{\frac{1}{2}} \qquad (1.26)$$

where τ_p is the Peierls stress, ρ_m is the mass density and b is the magnitude of the Burgers vector.

Potassium shows a rapid increase of critical flow stress with decreasing temperature.(38) For example, from 20K to 4K its critical shear stress increases by almost a factor of 2. This and other significant differences from fcc metals are ascribed to a limited mobility of the (a/2)<111> screw dislocation due to a high Peierls potential(38). In contrast to screw dislocations, edge dislocations in potassium do not feel the effect of a large Peierls potential and are

comparatively mobile(39). For this reason we expect deformations at 9K to produce more screw dislocations than edge dislocations; and for deformations at 60K, where the Peierls stress is less important, we expect to have more edge dislocations. Since screw dislocations are thought not to be pinned by impurities or vacancies due to their lack of a dilatational strain, we expect Eq.(1.26) is more viable for screw dislocations, and because edge dislocations are thought to be pinned by impurities or vacancies and not interact strongly with the Peierls potential, we expect Eq.(1.25) to be more viable for edge dislocations(6).

The inelastic interaction of these local modes in the phonon spectrum with the electrons was calculated by Gantmakher and Kulesco(33) who approximated the local modes by a single frequency—the Einstein oscillator. They found an additional electrical resistance due to such an interaction of the form:

$$\rho_{ed}(T) = (D/4T)\sinh^{-2}(\hbar\omega/2k_BT) \qquad (1.27)$$

where ω is the ground state frequency of the oscillator and D is a proportionality constant. Note that Eq.(1.27) predicts $\rho_{ed}(T) \propto T$ for $T \gg \hbar\omega/k_B$.

1.1.5 Electron-phason scattering and Charge Density Waves (CDW)

According to the CDW theory proposed by Overhauser(40), the

electron density in an alkali metal is modulated due to the electron-electron interaction:

$$\rho(r) = \rho_0 (1 + p\cos(\vec{Q}\cdot\vec{r} + \phi)) \qquad (1.28)$$

where p is the modulation amplitude, $\vec{Q}$ is the characteristic vector of the CDW ($Q \cong 2k_F$), and ϕ is an arbitrary phase term. The lattice then deforms sinusoidally in order to maintain overall charge neutrality. (The positive-ion lattice is approximated by a deformable-jellium model.) The wave vector $\vec{Q}$ is incommensurate with the reciprocal lattice vector $\vec{G}$. Since the presence of CDWs in potassium would change its nearly spherical Fermi surface into a complex interconnected one, this would have a profound effect on the transport properties of potassium. For example, the interconnected Fermi surfaces would reduce the magnitude of the minimum phonon wave vector q_{min} in the electron-phonon Umklapp scattering which would enhance such scattering. In addition the electron-electron Umklapp scattering would also be enhanced by another channel $\vec{K}_1+\vec{K}_2=\vec{K}_3+\vec{K}_4+\vec{Q}$ in addition to the original one $\vec{K}_1+\vec{K}_2=\vec{K}_3+\vec{K}_4+\vec{G}$. Therefore its contribution to resistivity is enhanced. This enhancement would also depend on the relative orientation of the electric field and the "Q" domains, which are defined as regions over which long range correlations of the CDW exist. The orientation of the "Q" domain is anticipated to be sample dependent, e.g. it can be changed by rapid cooling and deformation, and therefore the electron-electron scattering should also be sample dependent. According to Overhauser,

CDW's can have elementary excitations in which the phase ϕ varies periodically in time and space. These excitations are called phasons, and they behave differently from phonons as far as their dispersion relation is concerned. Using a phason-scattering mechanism Bishop and Overhauser(41) tried to explain the $T^{1.5}$ behavior in the resistivity measurement done by Rowlands et al.(24); but from the work done by Lee et al.(42), Black,(43) and Yu et al.,(27) we now know that the sample size can be responsible for the deviation from T^2 behavior in potassium samples thinner than 1mm.

Bishop and Lawrence(4) have combined the above-mentioned CDW electron-Umklapp scattering and phason scattering to explain the variability in A that Kaveh and Wiser tried to explain by electron-dislocation scattering. Bishop and Lawrence argued that different Q-domain textures could cause different amounts of phason and Umklapp contributions to $\rho(T)$. Since deformation could modify the Q-domain textures, our deformation studies have relevance to the CDW hypothesis. We were particularly interested in observing what small deformations might do to $\rho(T)$, which twisting the sample allows.

To identify the existence of CDWs in potassium has long been a subject of interest. Giebultowicz et al.(2), as we mentioned earlier, reported the observation of CDW satellites in their single crystal potassium sample by neutron diffraction. On the other hand, H. You et al.(3) reported recently that they failed to observe such satellites in their synchrotron X-ray diffraction experiments for their mosaic single crystal potassium. Indeed we need more experiments to positively

identify the existence of CDWs in potassium.

1.2 Thermoelectric Power S

From the basic transport equations given earlier

$$J = L_{11}E + L_{12}\nabla T \qquad (1.1)$$

$$\dot{Q} = L_{21}E + L_{22}\nabla T \ , \qquad (1.2)$$

we obtain the thermopower S:

$$S = (E/\nabla T)\big|_{J=0} = -L_{12}/L_{11} \qquad (1.29)$$

which is measured experimentally as follows: If we induce an infinitesimal temperature drop across the sample, there should be a thermoelectric voltage; and the thermopower is obtained if we divided this voltage by the temperature drop.

Theory predicts that the thermopower usually consists of two parts: the diffusion thermopower and the phonon drag thermopower.

1.2.1 Diffusion thermopower

The diffusion thermoelectric power contribution is usually associated with a system of electrons that interacts with a random distribution of scattering centers which are assumed to be in thermal

equilibrium at the local temperature T. As we will see in the next section, this assumption is a very poor approximation in the real situation; an additional contribution will appear when the assumption of local thermal equilibrium is lifted.

Assuming the conduction electrons constitute a degenerate Fermi gas, if one uses the relaxation time approximation, and if the higher order terms in the expansion of the Fermi-Dirac function are neglected, then one obtains the Mott(21) expression for the diffusion thermopower:

$$S = -\frac{\pi^2 k^2 T}{3e}\frac{\partial \ln \sigma(E)}{\partial E}\Big|_{E=E_F} \qquad (1.30)$$

where σ is the conductivity and E_F is the Fermi energy.

When impurity scattering dominates, one expects for potassium that $\partial \ln \sigma(E)/\partial E$ will be independent of temperature. Thus the thermopower in potassium should vary linearly with temperature T.

If there are two kinds of scattering processes involved in a system, for example, impurity scattering and dislocation scattering, and if Matthiessen's rule applies, then

$$\rho = \rho_i + \rho_d \ , \qquad (1.31)$$

where ρ_i and ρ_d are considered as independent impurity and dislocation contributions to the resistivity, respectively.

Using Eqs.(1.30) and (1.31), we have the Gorter-Nordheim relation(44) for the diffusion thermopower

$$S = (1/\rho)[\rho_i S_i + \rho_d S_d] = S_d + (\rho_i/\rho)[S_i - S_d] \qquad (1.32)$$

where S_i and S_d represent the diffusion thermopowers due to impurity scattering and dislocation scattering, respectively. Therefore, if we assume ρ_i is not changing during deformation and plot S as a function of $1/\rho$, we should get a straight line which intercepts the S axis at S_d.

1.2.2 Phonon drag thermopower

As we mentioned earlier, the assumption of thermal equilibrium in the calculation of the thermopower can be a poor one because the application of a temperature gradient across the sample causes the phonon distribution to go out of equilibrium. This phonon flow will "drag" the electrons to the end of the sample until the electric field formed by the piled-up electrons is large enough to stop further electron dragging. This will cause an additional thermopower term, the phonon drag thermopower.(45)

The phonon drag thermopower is usually divided into two parts: one due to the normal electron-phonon process and the other one due to the Umklapp process. The general theory in both cases tends to be rather complicated, but fortunately we will be working in the low temperature limit, $T < 1K$.

The normal process involves scattering of electrons within a

single Brillouin zone. In the low temperature limit this contribution to thermopower goes roughly as the lattice specific heat, which has a T^3 temperature dependence:

$$S_g^n \propto T^3. \tag{1.33}$$

The Umklapp process is more complicated. As we have seen earlier, a minimum phonon wave vector q_{min} is needed to scatter from one Brillouin zone to another if the Fermi surface does not touch the zone boundary, as in the case of potassium. We can estimate the number of such phonons to be proportional to $\exp(-\hbar V q_m/kT)$.

Guenault and MacDonald(46) fit their data to a simple equation of the form

$$S = S_0 T + BT^3 + C\exp(-\theta'/T) \tag{1.34}$$

where S_0T is the diffusion term, BT^3 is the normal electron-phonon drag term and $C\exp(-\theta'/T)$ is the Umklapp electron-phonon drag term. S_0 and B were found to be negative, and C was found to be positive, with $\theta' \sim 21K$. For temperatures lower than 1K the Umklapp term is usually negligible.

1.2.3 Thermoelectric ratio G

If we want to measure the thermopower, we must produce and measure

a temperature difference across the sample. Experimentally this turns out to be very difficult for potassium because it has a very high thermal conductivity, and it requires a huge heat flow across the sample to produce a large enough temperature difference for measurement. This heat flow usually exceeds the cooling power of the dilution refrigerator. Instead, the thermoelectric ratio G was actually measured in this work:

$$G = (J/\dot{Q})\big|_{E=0} = L_{12}/L_{22} \qquad (1.35)$$

From (1.1), (1.2), and (1.29), we know that the resistivity $\rho = 1/L_{11}$, the thermopower $S = -L_{12}/L_{11}$, and the thermal resistivity $W = -1/L_{22}$. So G can be written as

$$G = L_{12}/L_{22} = (L_{12}/L_{11})(L_{11}/L_{22}) = SW/\rho \qquad (1.36)$$

Since the Lorenz ratio L is defined as

$$L = \rho/WT \ , \qquad (1.37)$$

we have

$$G = S/LT \ . \qquad (1.38)$$

Now the thermopower can be related directly to the thermoelectric ratio

G. Ideally L should be a constant; and for T << 1K where elastic impurity scattering dominates, this is indeed the case where

$$L = L_0 = \pi^2 k^2/3e^2 = 2.445 \times 10^{-8}\ V^2/K^2 . \qquad (1.39)$$

From the results of Haerle et al.(47), we know that $L/L_0 = 0.97$ at 1K and that the ratio becomes even closer to 1 at lower temperatures. Since our interests are below 1K where the exponential Umklapp term is frozen out, G is expected to have the following simple form

$$G = G_0 + bT^2 \qquad (1.40)$$

where G_0 is the diffusion term and bT^2 is the normal phonon drag term. Any departure from this expression below 1K would indicate the presence of some other scattering mechanism which has not been taken into account in the above theory.

Chapter II Experimental Techniques

In this chapter, the major equipment used in the experiment will be described. Details will be given about the thermometry, the sample container, its functioning in deforming the sample, sample preparation, and the measurement procedures. In addition, possible heat flow problems and the measurement uncertainties will be discussed.

2.1 Main Equipment Used For Measurements

2.1.1 The dilution refrigerator

Since our emphasis on the properties of potassium is below 1K, a locally-built dilution refrigerator, which is capable of reaching 10 mK, has been used in the experiment. This dilution refrigerator was originally built by J. Imes and W. Pratt Jr.,(48)(49) and then modified by V. Heinen.(50) It can cool from room temperature to liquid nitrogen temperature in about 12 hours. It takes about 15 liters of liquid helium to reach 4.2K. The lowest temperature (about 10 mK) can be reached after 5-6 hours of $^3He-^4He$ mixture circulation. For a general description of a dilution refrigerator and its operation see Lounasmaa(51).

2.1.2 The high precision resistance bridge

As the discussion in section 2.6 will make clear, we measure $d\rho/dT$ in our experiments. For a typical unstrained potassium sample at 1K, the relative change of ρ, $\Delta\rho/\rho$, is about 10^{-5} with a temperature change of $\Delta T = 0.1$ K. Since $d\rho/dT$ is usually smaller at lower temperatures, rather precise measurements of $\Delta\rho/\rho$ are required. We have used a high-precision current-comparator system with a SQUID null detector. The system was built by D. Edmunds *et al.*(52) and can resolve the quantity $\Delta\rho/\rho$ to a precision of better than 0.1 ppm.

2.1.3 The screened room and floating pad

A commercial, double-layered screened room (from Erik A. Lingren and Associates, Inc.) surrounds the cryostat and screens out any radio-frequency noise which might affect the operation of the rf-biased SQUID. Since mechanical vibrations in the presence of the earth's magnetic field can induce currents which exceed the dynamic range of the extremely sensitive SQUID, the refrigerator body is magnetically shielded with high-μ metal and mounted on a vibration isolation table. All the pumps are kept outside the screened room and are connected to the refrigerator through flexible bellows.

2.1.4 A schematic diagram of the ultralow temperature part of the cryostat

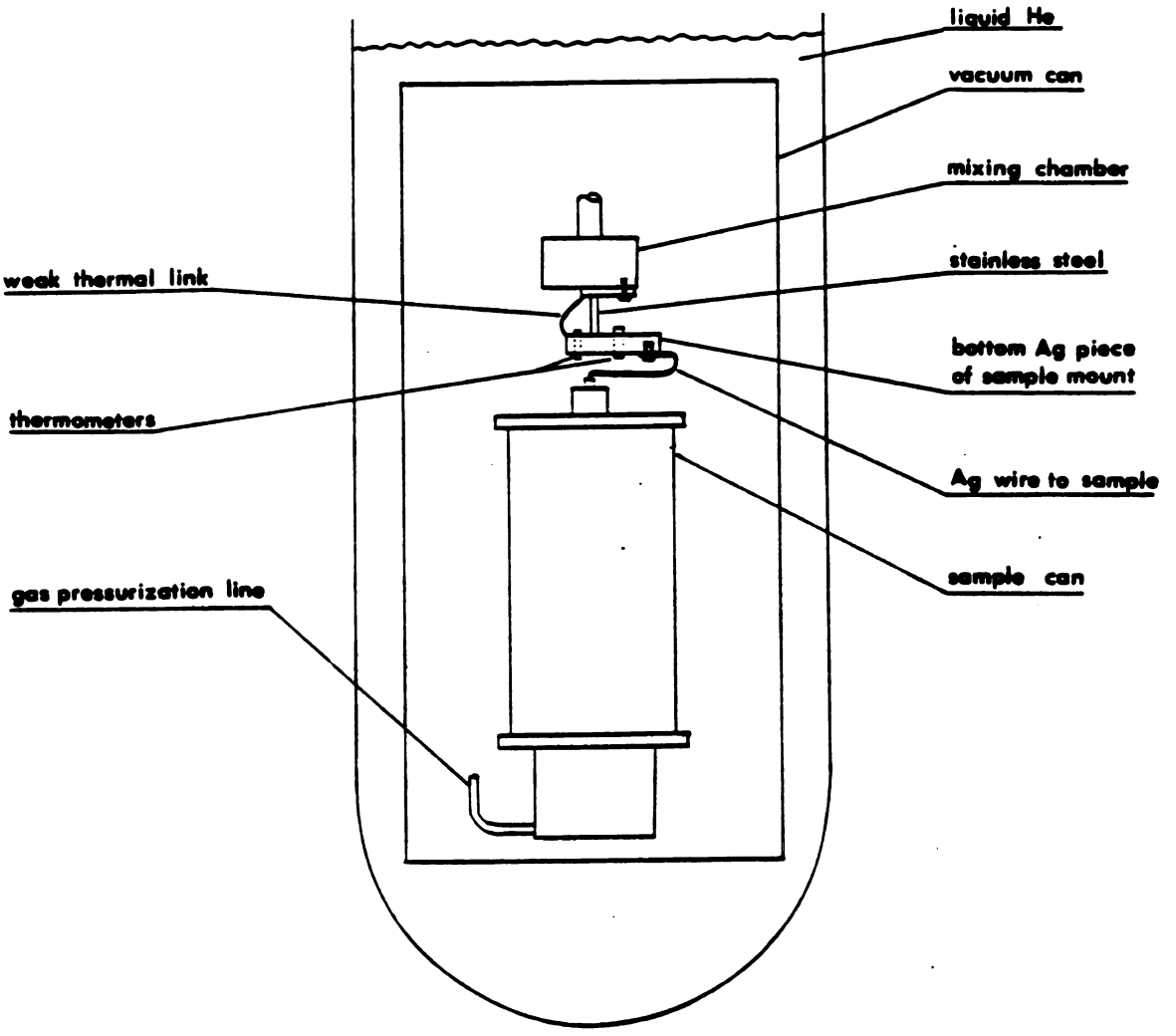

Figure 2.1
The low temperature part of the cryostat

Figure 2.1 shows the low temperature part inside the cryostat. The details will be discussed in later sections.

2.2 The thermometry

The temperature was measured in this experiment with two germanium resistance thermometers and one Cerrous Magnesium Nitrate(CMN) susceptibility thermometer. The calibration of these thermometers was done by C.W. Lee and V. Heinen et al.(50) The two germanium resistors are mounted in the holes in the bottom piece of the sample mount using Apiezon N grease for thermal contact. The susceptometers of the CMN thermometer are mounted against and thermally isolated from the plastic wall of the mixing chamber. Silver wires of 1-mm-diameter provide thermal contact between the bottom piece of the sample mount and both the CMN sensor and its susceptibility coils.

For temperatures above approximately 1.5K, "R6" is used, which is a Lakeshore Cryotronics germanium resistor. The calibration was done as follows: First, the susceptibility of a CMN sample was measured against SRM767 and SRM768, which are the superconducting fixed point devices from the National Bureau of Standards. Since the susceptibility of CMN is proportional to T^{-1} over the temperature range of interest here, temperatures other than the fixed points could be easily determined by interpolation. Then by using a least-squares fit, the resistance of R6 was fit to the temperatures given by the CMN for temperatures between

1K and 4.2K using the following equations

$$\text{Log } T = \sum_{n=0}^{N} a_n (\text{Log } R)^n \qquad (2.1)$$

$$\text{Log } R = \sum_{n=0}^{N} b_n (\text{Log } T)^n \qquad (2.2)$$

with N = 7. With these fits, the temperature given by R6 is estimated to be within 0.3% of the absolute temperature.

For temperatures between approximately 40 mK and 1.5K, "R7" is used, which is a Cryocal CR50 germanium resistor. The method of calibration was similar to that used for R6, except that the susceptibility of an irregular single crystal of 10% CMN and 90% LMN(Lanthanam Magnesium Nitrate) was used for interpolating between the fixed points. The resistance of R7 is fit to the temperatures given by the susceptibility of the CMN-LMN using the equations given above with N=9. The error is estimated to be within 0.7% of the absolute temperature.

Below approximately 50 mK the CMN thermometer is used which consists of a susceptometer (Fig. 2.2) and a CMN pill. The CMN pill is a 50:50 volume mixture of CMN and 700-Å Ag powder pressed onto a 0.012" diameter Ag(0.4 at% Au) wire. The pill is a right circular cylinder (height=diameter=1/8") containing approximately 18 mg of CMN and 95 mg of Ag. The Ag(Au) alloy wire is used to reduce any possible eddy currents caused by the 17 Hz magnetic field used to measure the susceptibility. The eddy currents can produce fields which would affect the measured susceptibility and could also cause heating of the CMN

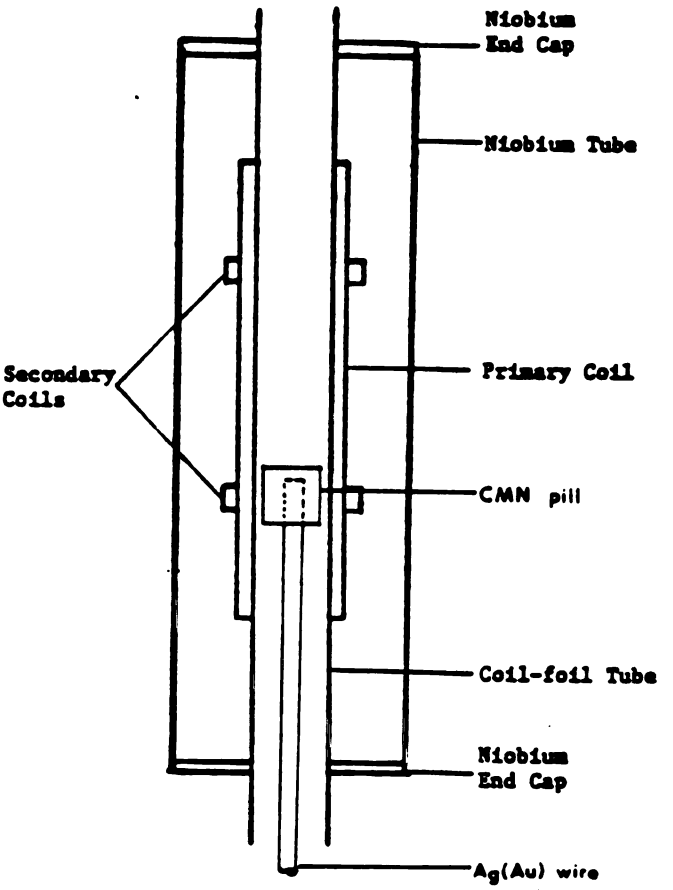

Figure 2.2
The CMN thermometer

pill. This wire is approximately 1" long and is spotwelded to a pure Ag wire which is attached to the bottom Ag sample mount. For a more detailed description of the CMN thermometer see V. Heinen's Ph.D. thesis.(50)

The CMN thermometer was calibrated against the SRM 768 which is the low temperature standard. It has the following fixed points: W (15.5 mK), Be (22.92 mK), Ir (99.13 mK), AuAl (160.43 mK), and AuIn (204.36 mK). The 22.92 mK point has not been used because this superconducting transition point was in complete disagreement with the other fixed points. A linear least-squares fit has been done to the 15, 99, 160, and 204 mK points assuming a Curie law behavior for the susceptibility of the CMN. In the overlapping temperature range of the CMN thermometer and R7, the temperature difference was found to be less than 1%.

We have used two thermometers for temperature regulation of the mixing chamber. A carbon resistor is used as the temperature sensor for $T \gtrsim 50$ mK. The other sensor is a second identical CMN thermometer, used for $T < 50$ mK, since CMN has a much better temperature response in this range. This system has the unique feature that only one SQUID is used as the null detector for both CMN mutual inductance bridges. Figure 2.3 shows how this is done. Two independent AC oscillators, V_1 and V_2 , drive the two bridges. Each Intersil #ICL 8038 sine wave generator is powered by a separate 6V battery, one operates at 17 Hz and the other at 40 Hz. Their maximum output is 1 V p-p. There is also an optical coupler output for the reference channel of each lock-in

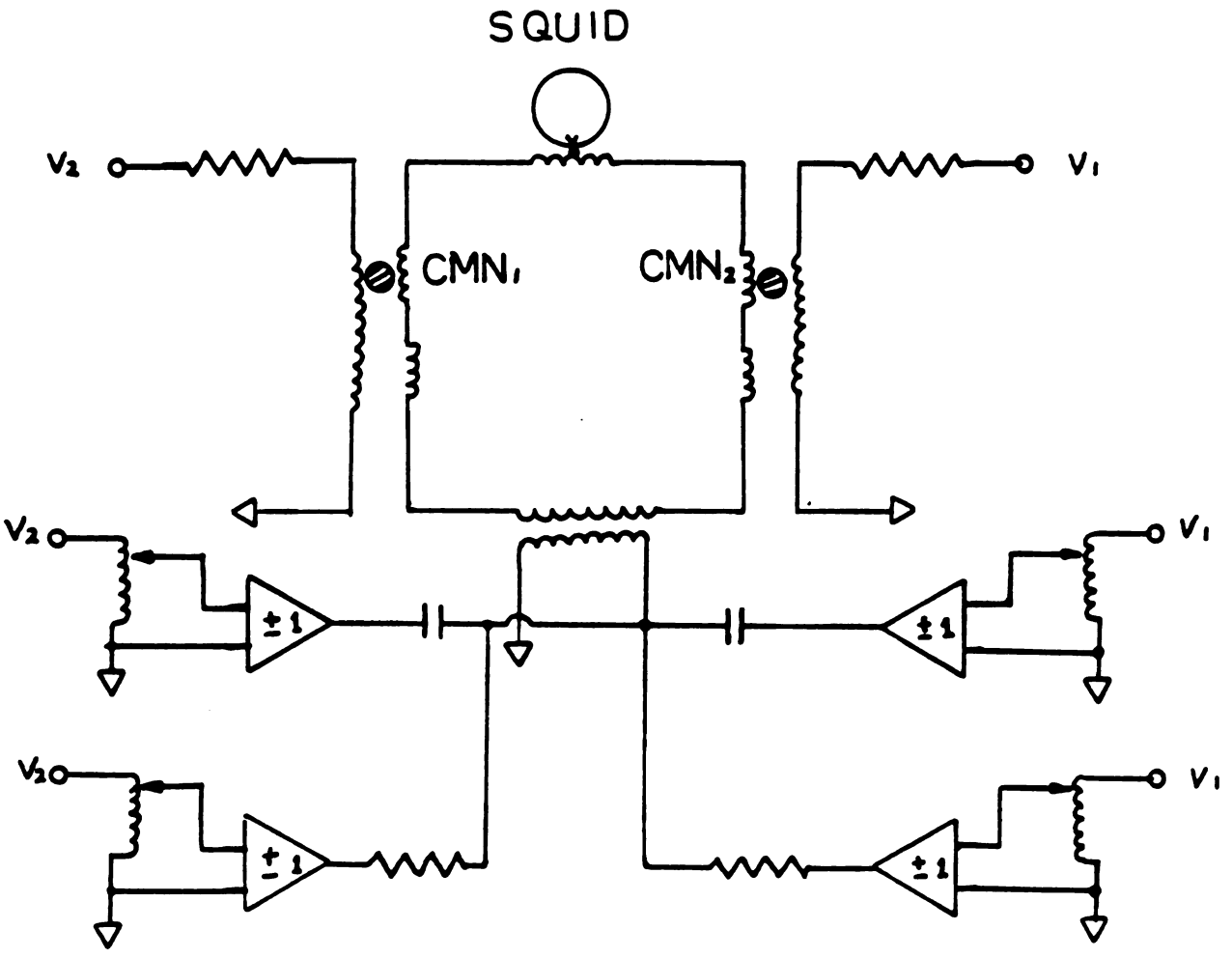

Figure 2.3
Circuits of the CMN mutual inductance bridges

amplifier. Two HR-8 lock-in amplifiers from Princeton Applied Research Corp. are used to independently extract the two AC signals at the SQUID output. No interference between these two CMN bridges has been observed in this experiment.

Also a silicon diode thermometer from Lake Shore Cryotronics, Inc. is used for determining the temperatures above 4.2K during twisting and annealing of the sample. This thermometer is thermally connected to the top end of the sample. The voltage across the diode is measured with 10 μA reversed biased current.

2.3 The sample can

Since potassium reacts with oxygen and water vapor, a self-contained sample can has been used which permits both our measuring the electrical properties of the sample and deforming the sample at low temperatures.

Figure 2.4 shows a drawing of the sample can which is capable of twisting the sample while mounted on the dilution refrigerator. The sample can and dilution refrigerator are both mounted inside a main vacuum can, which is surrounded by liquid helium, as shown in Fig. 2.1. The sample can can be separated into three assemblies: The top flange D on which the feed-throughs B and the sample holder H are mounted, the central body cylinder F, and the bottom flange P on which the twister is mounted.

The three assemblies are sealed together by two replaceable indium

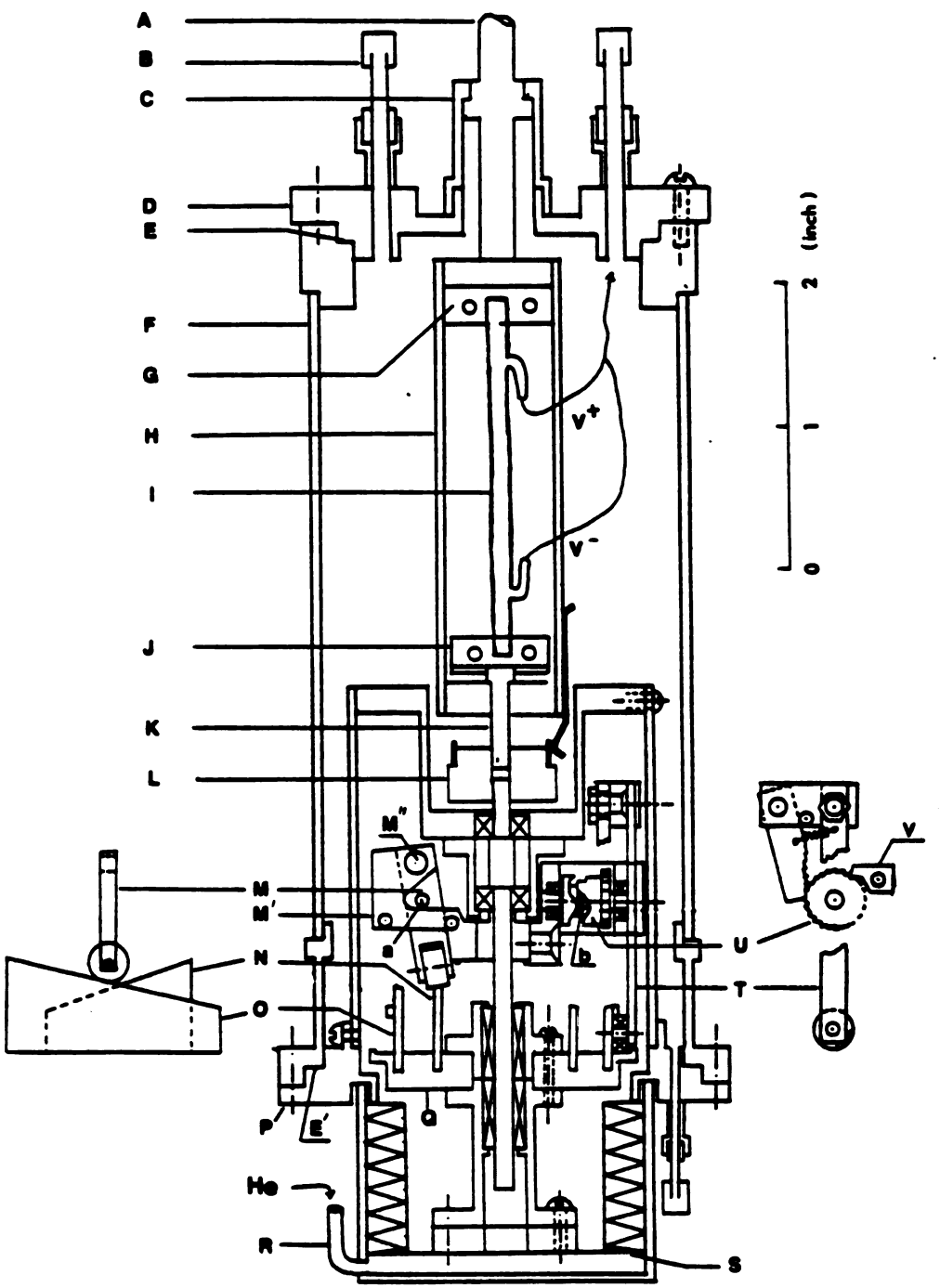

Figure 2.4
The sample can

Table 2.1 A list of parts in sample can (shown in Figs. 2.4 - 2.6, not all parts are shown in each figure)

A	central rod	S	bellows
B	feed-through	T	pulling gear bar
C	central rod housing	U	ratchet cam
D	top flange	V	pawl
E	top indium 'O' ring	W	pushing bar
E'	bottom indium 'O' ring	a	flipper pin hole
F	central body cylinder	b	ratchet cam pin
G	top sample mount		
H	nylon sample holder		
I	potassium sample		
J	bottom sample mount		
K	twisting shaft		
L	torque coupler and rotation detector		
L'	twisting key		
L"	rotation detector		
M	flipper		
M'	flipper arm		
M"	flipper axis		
N	inner track		
O	outer track		
P	bottom flange		
Q	track housing		
R	pressurizing line		

"O" rings located at E and E', respectively. After the sample is mounted, the top flange E is sealed last while the can is still inside the argon glove-box. Then the whole can is taken out of the glove-box and mounted underneath the mixing chamber of the dilution refrigerator.

The top flange is made of brass. On it there are the central rod A and two feed-throughs B. A is made of OFHC copper and is epoxied onto a housing C, which is made of "Vespel" (SP-22 Polymide, from Dupont, Inc.), a very good heat insulator at low temperatures. The rod serves as both the heat path and one of the current leads of the sample. One of the feed-throughs B is used for various electrical leads, and the other one is used as a safety valve, made by soldering a thin brass foil onto it. The central body cylinder F is made of copper to which the two upper and lower flange housings are hard soldered. There is a heater (not shown in the figure) mounted on the outside of the cylinder to control both the deforming and annealing temperatures. The lower flange assembly P consists of the bellows and the twister systems, and their functions will be described in the following section.

Figure 2.5 is a perspective drawing of the sample holder H, which is made of nylon. The two sample mounts, G and J, are made of OFHC copper, and G is part of the central rod A. The lower sample mount J can be turned by the torque coupler L, which is also made of "Vespel". The coupler is driven by key L', which is on the output shaft of the twister. The current is run through A and J, and the voltage is picked up through the V-probes in the figure. A heater is mounted on the back

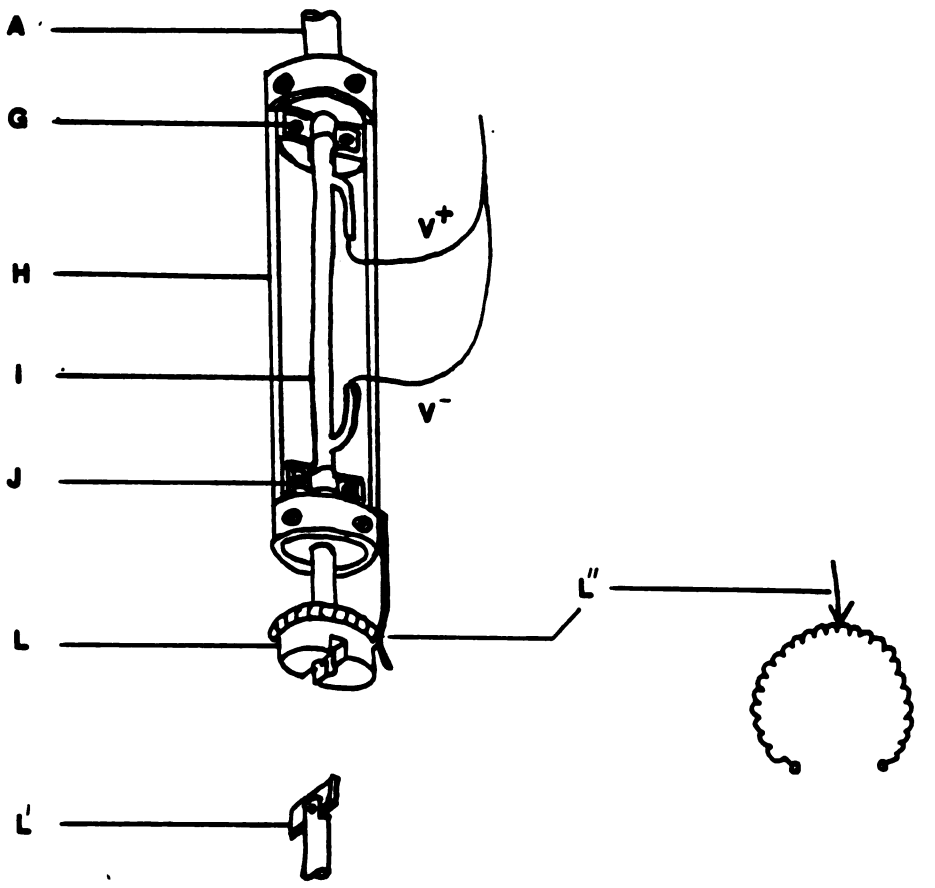

Figure 2.5
A perspective view of the sample holder

side of J for the thermoelectric ratio G measurements (not shown in the figure). Note a potentiometer L" is mounted on the torque coupler so that the angle through which the sample is twisted can be read.

2.4 Plastic deformation of the sample

The main feature of the twister is as follows: At any temperature above 4.2 K, if we apply about 30 psi pressure of helium gas to the bellows S, we can obtain a maximum torque output through L' of about 5 pound-inch, which will twist potassium samples of 3mm diameter through about ±80 degrees. The direction of twist can be chosen at will and twisting only occurs during the upward power stroke of bellows S. To obtain a larger amount of deformation, one has to twist the sample back and forth many times. Since the SQUID circuit is very sensitive to stray magnetic fields, a purely mechanical method of setting the direction of twist has been used, rather than the more obvious electro-mechanical method.

The detailed description of this twister can be understood either from Figure 2.4 or the simplified perspective drawings Figures 2.5 and 2.6.

Inside the twister there is a flipper M at the bottom of which is a wheel. This wheel can sit at a position above either the inner track N or the outer track O. When the tracks, together with their housing Q, are driven up by the pressurized bellows, one of the tracks will hit the wheel and force it to move along the slope. Since the attached

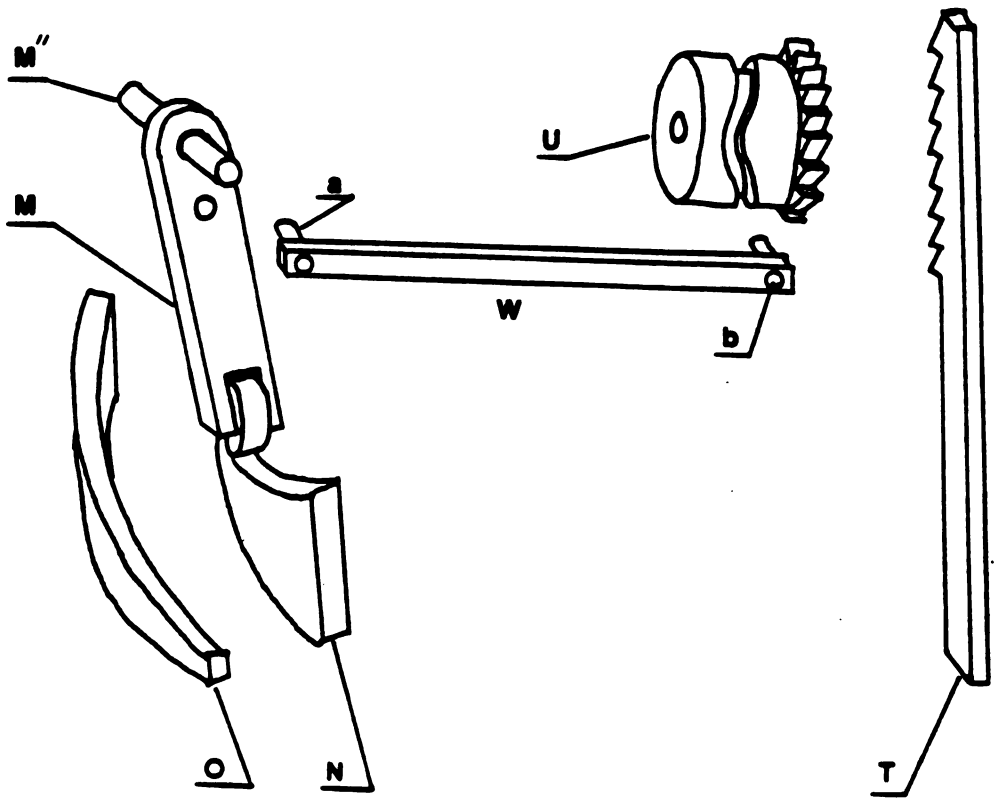

Figure 2.6
A perspective drawing of the twister mechanism

flipper is connected via M" and M´ to the central shaft, this motion will force the central shaft (with key L´ at its top) to turn through an angle. If the flipper sits above the other track which has the opposite slope, L´ will turn in the opposite direction.

There is a gear arm T attached to the housing of the tracks Q. When the pressure inside the bellows is lowered, the housing will return to its lower position. On its way back the gear arm T will turn the ratchet cam U. Note that there is a curved groove in the ratchet cam U, and pin b is engaged in it. When U turns, the curved groove will force the pin b and hence bar W to move horizontally, which will bring the flipper to the other position. When T rises, a pawl V keeps U from turning. Usually several small up and down motions of T are required to switch flipper M between tracks. During these oscillations of T, the flipper M does not contact the track. Thus the sample is not twisted.

When the bellows is driven up again by pressurized helium gas, the central shaft this time will turn in the opposite direction. Thus a back and forth rotation is accomplished. In addition to the rotation detector, two similar position detectors have been put inside the twister to detect the actual position of the bellows and the actual position of the flipper(not shown in the Figures).

The He gas in the bellows must be isolated from sample area inside the can because any helium gas there would provide a heat path between the sample and the wall of the sample can. The residual argon gas brought from the argon glove-box is solidified at helium temperature.

The plumbing for the pressurization system connected to the bellows is shown in Figure 2.7, which is similar to that of Haerle's.(47) Normally when operating the bellows valve #1 is closed and helium is slowly applied through valves #2 and #3. The two-line system has been built for the following reasons: If a solid air plug should form when pressurizing at around 10K, the bellows could still be evacuated by using the second line because any plug would take place in the first line above the liquid helium level, which would be above the place where the two lines joined to form one thin line going into the vacuum can. The ballast tanks are about 10 cubic inches in volume and are used to damp out any Taconis oscillations.

2.5 Sample preparation

The samples were prepared inside a commercial argon glove-box (Vacuum Atmosphere Company) with the gas purifying system built locally. In comparison with another VAC helium glove-box having a nominal oxygen contamination of less then 0.4 ppm, the time that potassium remained shiny inside the argon glove-box was longer or equal to that of the potassium inside the helium one. So we know that the oxygen concentration inside the argon glove-box is less than or equal to 0.4 ppm. The water vapor content has not been directly measured but exposed potassium remains shiny for hours. In order to allow the sample can to outgas and the purification system time to remove any residual contamination brought in with the can, all needed materials were placed

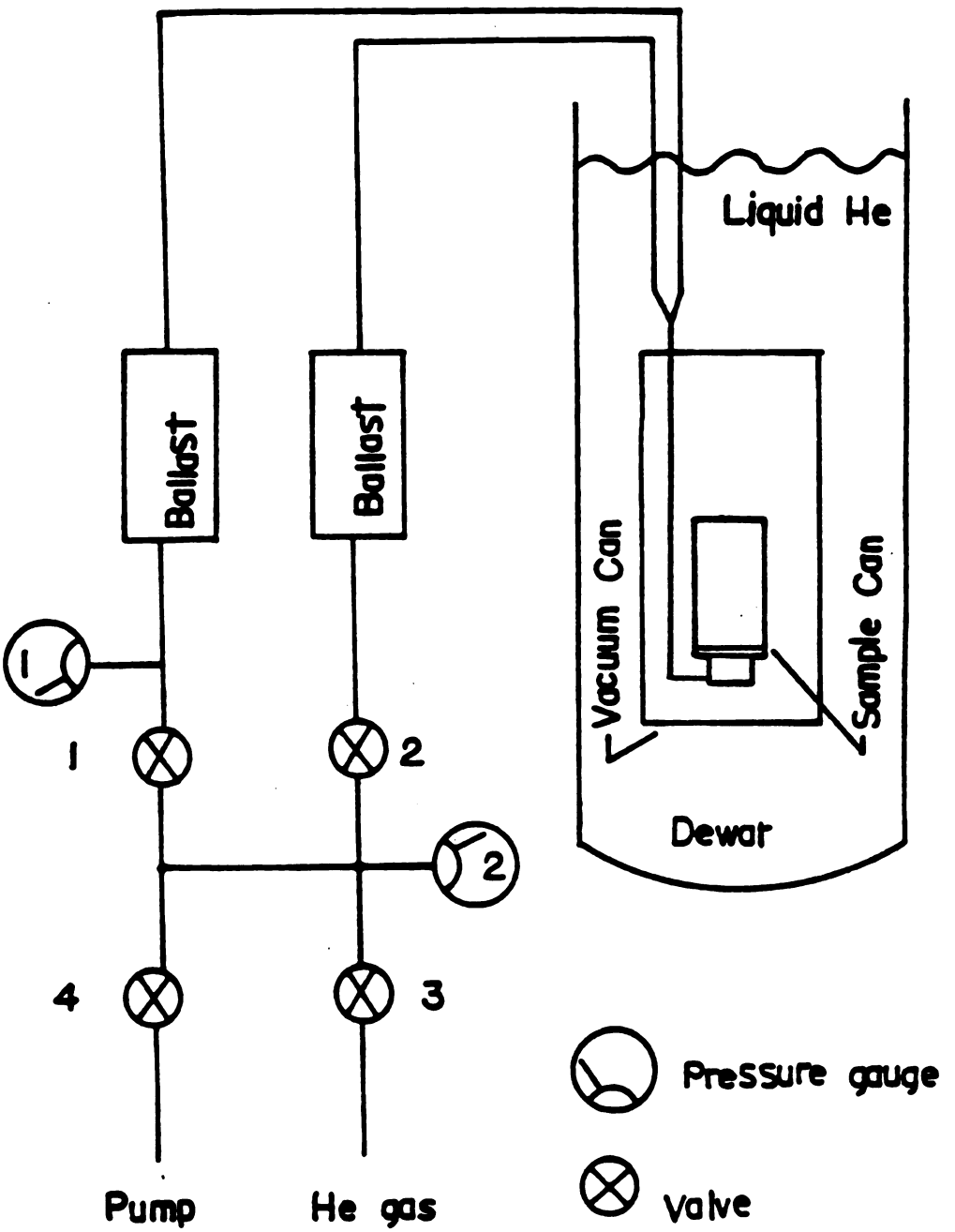

Figure 2.7
The He pressurization system for the bellows

in the air-lock and pumped on for at least 24 hours. Then they were placed in the glove-box for another 24 hours before the sample was made. To further reduce the contaminants inside the can, an oxygen getter was used. Before the can was closed, a thin copper sheet about 2"x7" in size was smeared on one side with a thin layer of K or Rb and then placed inside the can with the unsmeared side against the inner surface of the can body. In this way the sample surface remains reasonably shiny even after a run of several weeks. It is very important that the sample surface remain clean since thick deposits of K compounds on the sample surface have been observed to significantly alter the mechanical properties of the sample.

The pure potassium sample is made of 99.95% potassium obtained from Callery Chemical Company, a division of Mine Safety Appliances Company. Table 2.2 shows the chemical composition of a similar batch of the potassium. The potassium came in glass ampoules sealed under argon gas. The ampoules were opened inside the glove-box, and the potassium was melted and transfered to the stainless steel press (Figure 2.8). If the sample was K(Rb) alloy, the potassium was first melted and poured into a hot glass beaker; and then some Rb was melted into the beaker before the alloy was poured into the press.

The samples were extruded through a 2mm diameter die. The samples were about 40mm long between the voltage probes (Figure 2.4) and were cold welded onto the copper mounts J and G which had been smeared with some potassium first. Then the sample ends were clamped onto the mounts by two previously potassium-smeared copper clamps. This assures that

Table 2.2 Chemical analysis of potassium

Element	PPM	Element	PPM	Element	PPM
Fe	<5	Cr	<5	Sr	<1
B	<10	Si	25	Ba	<3
Co	<5	Ti	<5	Ca	8
Mn	1	Ni	<5	Na	15
Al	<2	Mo	<3	Pb	<5
Mg	2	V	<1	Zr	<10
Sn	<5	Be	<1		
Cu	<1	Ag	<1		

This information is from the Callery Chemical Company.

< means less than this level of impurities could not be detected.

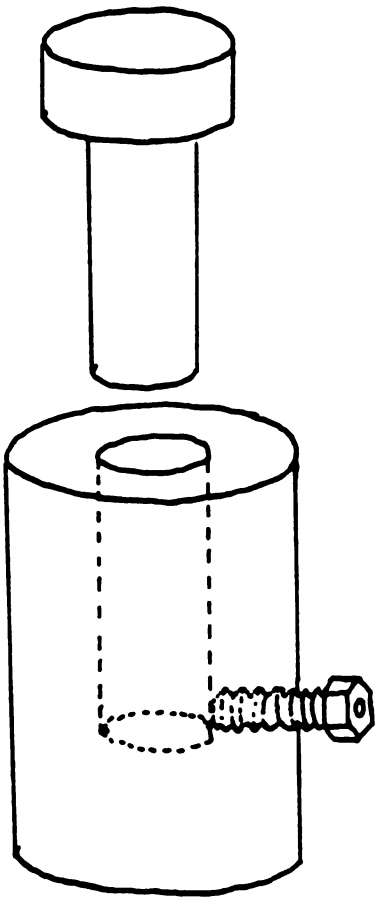

Figure 2.8
The press and die for extruding the sample

we do have good mechanical and electrical contact between the sample ends and sample mounts. Next, two potential probes of the same potassium were extruded and cold welded onto the sample and then attached to two 2x3 mm Ag tabs on which fine superconducting Niomax wires had been soldered beforehand. Since potassium is very sticky at room temperature, we have had no trouble with these cold-welded joints. The fine superconducting wires are the voltage lead connections to the SQUID circuit, and they are sufficiently flexible that negligible torques are applied to the sample by them during twisting.

Before mounting the can onto the dilution refrigerator, the room temperature resistance of the sample is measured by passing a known current through the sample and measuring the resulting voltage across the sample with a Keithley 180 nanovoltmeter. After the can is mounted, the bellows pressurization line is connected and leak tested. Then a small angle twist is made to ensure that every thing is working. This twist would introduce no dislocations because all the dislocations and vacancies anneal out at room temperature(10). Finally the bellows is evacuated and left in this state until the first deformation of the sample is to be performed.

2.6 Measurements

This section is intended to explain how the various parameters of the samples are measured.

The ratio of the cross sectional area to the length of the sample,

A/L, is measured before and after the run to make sure that the sample geometry does not change during deformation of the sample.

Since A/L is given by

$$A/L = \rho(300K)/R(300K), \qquad (2.3)$$

we just measure the resistances before and after the run and compute the ratio

$$r = \frac{R(300K)_{before}}{R(300K)_{after}} \qquad (2.4)$$

which would tell us if the sample geometry has changed, since $\rho(300K)$ is a constant. Results show that the change is less than 1%, which is much better than the previous work of Haerle (<10%).

Once the sample is cooled to 4.2K or lower, the circuit shown in Figure 2.9 is used. This low temperature circuit consists of the SQUID (Superconducting Quantum Interference Device) null detector and two resistors wired in series. The two resistors are 1) R_k, which is the potassium sample, and 2) R_r, which is a Cu(Ag) alloy resistor designed to have a resistance with small temperature and current dependences. The wires connecting these resistors are made of Niomax CN, a multi-filament Nb(Ti) superconducting wire with Cu(Ni) cladding from Imperial Metal Industries(potential leads), and the T48B superconducting wire from Supercon, Inc., with about 1 cm of the copper cladding etched off for thermal isolation(current leads). To minimize

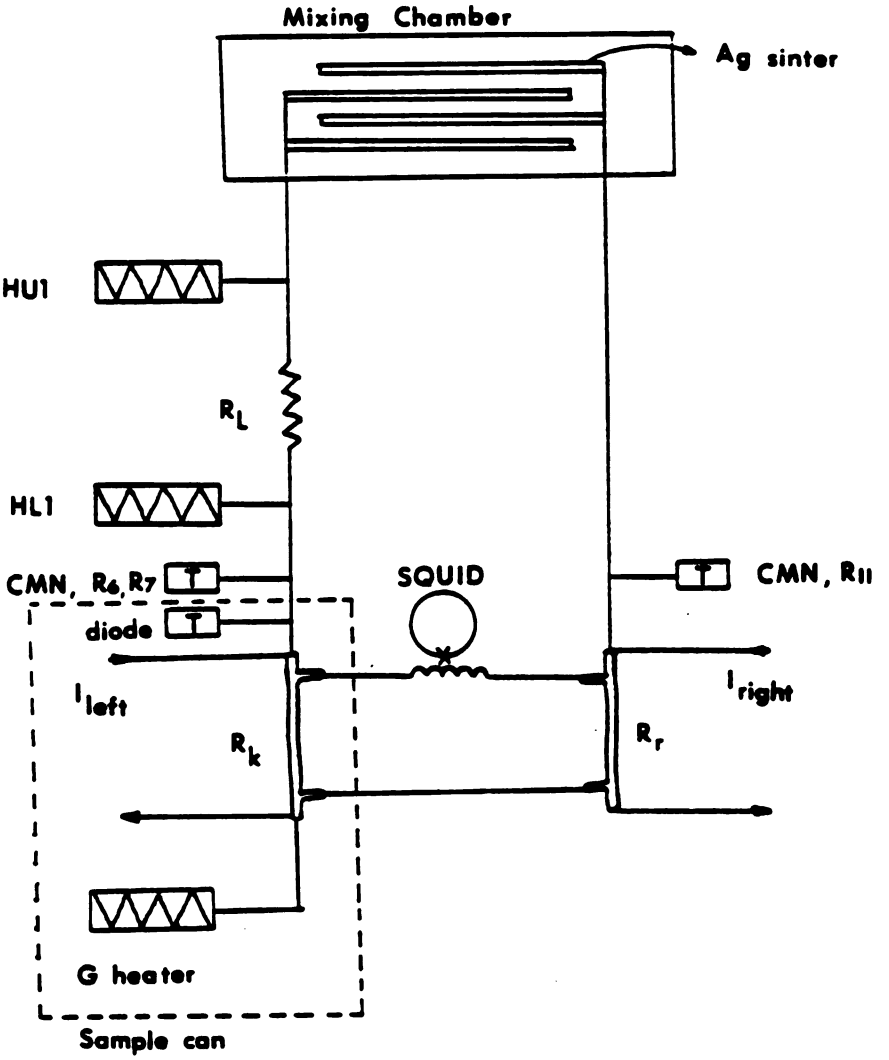

Figure 2.9
The low temperature circuit

the noise introduced by stray magnetic fields, most of the wires except those near the sample are shielded in superconducting lead tubing. The wires leading to the sample are all carefully tied or varnished down to reduce magnetically induced currents and heating due to vibration.

The wires exit the can through electrical feed-through B (Figure 2.4). This feed-through is made by running the superconducting wires through a clean stainless steel tube which is then inverted in a cup of Stycast 1266 epoxy.

Two reference resistors have been used in the experiment, and they are all made of oxygen-annealed dilute Cu(Ag) alloys. One of them was made by Haerle (47), had a 4.2K resistance of about 1.6 $\mu\Omega$ and was used for the K(Rb) alloy sample. The other one was made in a similar manner, had a 4.2K resistance of 0.18 $\mu\Omega$ and was used for the pure K sample.

The resistance ratio C can be measured by using the current comparator together with the SQUID as the null detector mentioned in 2.1.2. The current comparator generates two currents, I_m and I_S , with the ratio $C = I_S/I_m$ being stable to a 0.1 ppm precision. When comparing resistances, one current I_m passes through what is called the master side resistor R_m , and the other current I_S passes through the slave side resistor R_S. The master side current I_m can be ramped slowly to a predetermined value. The current I_S is $C \cdot I_m$ where C is the switch setting of the current comparator. C is adjusted until the SQUID output signal indicates a null condition at its input.

The thermal EMFs generated in the circuit can be eliminated by the

following procedure. Let V_S be a stray voltage in the circuit due to a thermal EMF. Then for the currents going in one direction the SQUID measures

$$V(+) = I_S R_S - I_m R_m + V_S \ . \qquad (2.5)$$

When one reverses the currents, one has

$$V(-) = -I_S R_S + I_m R_m + V_S \ . \qquad (2.6)$$

Since C is adjusted until V(+)=V(-), one has

$$I_S R_S - I_m R_m + V_S = -I_S R_S + I_m R_m + V_S . \qquad (2.7)$$

Finally one obtains

$$I_S/I_m = R_m/R_S = C \qquad (2.8)$$

which is independent of V_S.

We now show how one can obtain the temperature derivative of the resistivity by measuring the ratio C. One possible procedure would be to keep the reference resistor at 4.2K and measure C as the sample temperature is varied. The disadvantage of this method is that the Johnson noise generated by the resistor at 4.2K is much larger than at 40mK. To minimize this noise one would like to cool the reference to

the same temperature as the sample, but then there is a problem of separating its temperature dependence from that of the sample. This can be solved in the following way: We regulate the reference temperature (T') while applying steady heat to upper heater 1 (Figure 2.9, HU1), and we measure the ratio C at temperature T. Next we switch the heat to HL1 so that a temperature difference ΔT is produced across R_L, a Ag(Au) resistor of about 50 $\mu\Omega$. Then we measure $C + \Delta C$ at $T + \Delta T$. We want to calculate the quantity

$$C/(C\,\Delta T)\ . \tag{2.9}$$

Let us define

$$C = R_k/R_r\ . \tag{2.10}$$

After the sample temperature is raised the reference temperature is still kept at the same temperature T'. Therefore one has

$$\Delta C = \Delta R_k/R_r\ , \tag{2.11}$$

or

$$(1/C)\Delta C/\Delta T = (1/R_k)\Delta R_k/\Delta T. \tag{2.12a}$$

If ΔT is small enough, this leads to

$$(1/C)\Delta C/\Delta T \Rightarrow (1/\rho)d\rho/dT = (1/\rho_o)d\rho/dT \ . \qquad (2.12b)$$

Below about 1K, the right hand part of (2.12b) is obeyed since the total variation of ρ below 1K is about $\Delta\rho/\rho = 10^{-4}$. Therefore $d\rho/dT$ can be obtained by multiplying (2.12b) by ρ_o in the plots of the data.

One advantage of this temperature-modulation method is that we can double-check our thermometry here. As mentioned above, we know the amount of heat $\dot{Q}$ being put into the heaters HU1 and HL1 in order to produce a temperature difference ΔT across R_L, the Ag(Au) resistor in Figure 2.9. The Wiedemann-Franz law states that

$$R_L/W = L_oT \qquad (2.13)$$

where R_L is the resistance, $W = \Delta T/\dot{Q}$ is the heat resistance and L_o is the Lorenz number. We obtain that

$$R_L = L_oT\Delta T/\dot{Q} \ . \qquad (2.14)$$

If our thermometry were perfect, the value of R_L we calculate at different temperatures using (2.14) should be a constant. Thus we check our thermometry by calculating R_L occasionally during our runs. We usually measure R_L at T = 0.03, 0.05, 0.15 and 0.6K during each run. For example, in our run with sample K-1 the average of R_L was 46.65 $\mu\Omega$ and the standard deviation was 1.1%; In our run with K-5 the average of

R_L was 46.5 $\mu\Omega$ and the standard deviation was 2.6%. The overall standard deviation of R_L in each run was less than 3%.

The current put through the sample is usually 50mA, but occasionally checks are made to be sure that there is no current dependence by using 25mA.

Another quantity measured in the experiment is G, the thermoelectric ratio. G is defined as the ratio of the electrical current to the heat flow at zero voltage drop across the sample:

$$G = I_g/\dot{Q}|_{E=0} = I_g/I_h^2 R_h \qquad (2.15)$$

where I_g is the current passing through the sample to counteract the thermal voltage resulting from the heat flow through the sample: $\dot{Q} = I_h^2 \cdot R_h$. I_h is the G heater current, and R_h is its resistance.

The measurement is done as follows. First we pass a known heat flow $\dot{Q}$ through the sample, and this causes the SQUID to go off the null value because a thermal voltage is generated. Then we put a balance current I_g through the sample by adjusting the dials on the current comparator until the SQUID indicates the null condition again. No currents passed through R_r during these measurements. Then from (2.15) the G value is obtained.

2.7 Heat loss

It is important that all the thermometers which are mounted on the

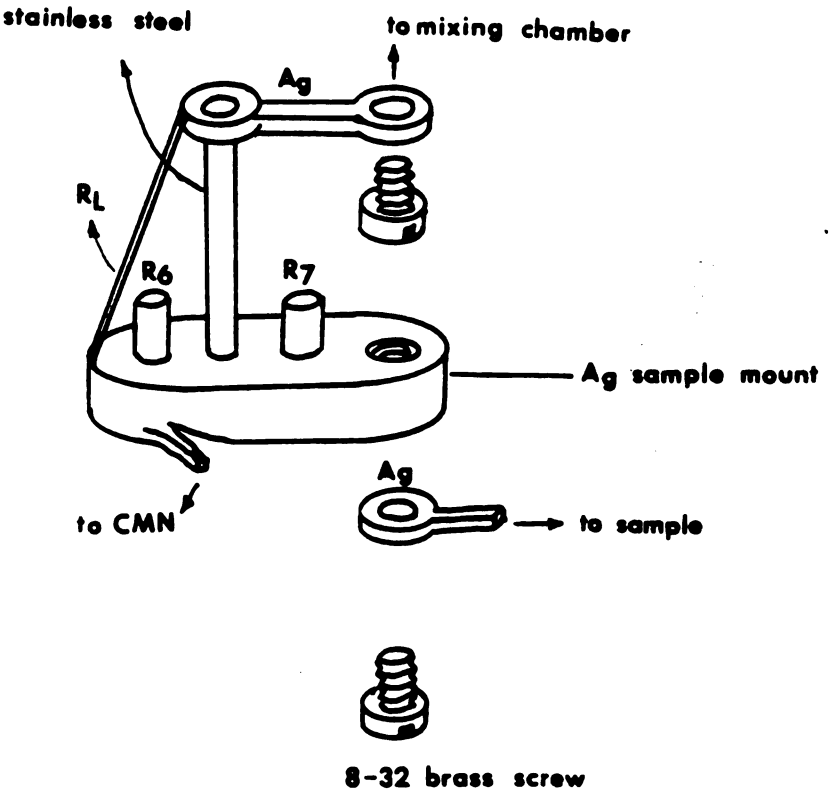

Figure 2.10
The Ag sample mount
The Ag sample mount on which the thermometers etc. are mounted

silver sample mount (Fig. 2.10) be at the same temperature as the sample. Thus any heat flow between the sample and this sample mount must be kept to a minimum level. The heat losses due to the superconducting leads are negligible since they are very poor heat conductors at these low temperatures.

Since the body of the sample can is directly attached to the mixing chamber by a Ag wire, any heat paths to the can from the sample will be considered to be heat leaks. From Fig. 2.4 we see two such paths. One path is via the central rod housing C, and the other is via the torque coupler L. They are both made of "Vespel". The empirical formula for its thermal conductivity at low temperature is

$$K = 17\ T^2\ \mu W/(cmK). \qquad (2.16)$$

We want all the heat generated by heater HL1 to flow only through the weak thermal link R_L (Figs.2.1, 2.9, 2.10), which is a Ag(Au) wire with a resistance of $\sim 50\ \mu\Omega$. By using the Wiedemann-Franz law, we know that the thermal resistance of this wire is about 2×10^3 (K/Watt). The thermal resistance of the housing C is therefore designed to be about 10^5 (K/Watt), roughly 50 times that of R_L at 1K. The bottom sample mount J is made of OFHC copper and is hard soldered to a stainless steel shaft K. The heat loss due to the torque coupler L is estimated to be much less than that of the housing C.

The electrical resistance from the top sample mount G to the silver tab (Fig. 2.10) was measured to be less than 2.4 $\mu\Omega$ at 4.2K, the

estimated temperature difference between the sample and the thermometers is less than 0.2 mK for the worst case (at 1K).

2.8 Heat generated while deforming the sample

As we mentioned in Chap. 1 (Section 1.1.1 and 1.1.4), for temperatures near 10K, the actual temperature at which the sample was deformed must be known since screw dislocations appear to rearrange themselves near 10K and vacancies begin to anneal out above 10K. It is therefore necessary to calculate the temperature increase while the sample is being twisted. Unfortunately, we do not have a thermometer mounted directly on the sample. However, the diode thermometer is mounted nearby on the top sample mount (Fig. 2.9) to which the sample is cold welded. First let us calculate the heat relaxation time τ of the sample. We know that the temperature distribution function $U(x,t)$ for a bar of length L is of the form

$$U(x,t) = \sum_{n=0}^{\infty} C_n e^{-\frac{t}{\tau_n}} \sin\left(\frac{n\pi x}{L}\right) \qquad (2.17)$$

where the relaxation time τ_n is defined as

$$\tau_n = (L/n\pi)^2 1/a^2, \text{ and} \qquad (2.18)$$

where L is the length of the bar and $a^2 = k/c\rho$ in which k is the thermal conductivity, c is the specific heat and ρ is the mass density.

For potassium at 10K, we have k=4.0 Watt/cmK, c=0.07 Joule/gK and ρ=0.86 g/cm^3 . Therefore we have

$$\tau_1 = 0.034 \text{ sec} , \qquad (2.19)$$

which is the longest relaxation time in τ_n. Our twist is typically done in about 1 second, which means that the whole sample is at a uniform temperature during most of the deformation if, as a worst-case example, we assume no heat is flowing out of the ends of the sample.

Now let us calculate the work needed to twist the potassium sample. The yield stress σ for potassium at 10K is about 1 Kg/mm^2 (57) and according to Cottrell(58), the torque T' needed to twist a bar of radius r and shear stress σ is

$$T' = (\pi/2)r^3\sigma. \qquad (2.20)$$

For our sample we have r=1mm, therefore we get T'=1.57 (kg-mm). If we twist the sample by π, the work done is $\sim$ 0.05 Joule. The specific heat of potassium near 10K is 0.07J/gK, and the sample mass is about 0.15 g. Thus the temperature increase due to this heating is

$$\Delta T \cong 5 \text{ K} . \qquad (2.21)$$

The actual temperature increase is much less than this because the sample is in contact with the sample mounts which have a much bigger

heat capacity. For example, let the total heat of deformation flow through the whole sample and out of the upper end which is in contact with the central rod. Since $\tau << 1$ sec, we can assume that a uniform temperature gradient is rapidly established across the sample and obtain for the temperature drop across the sample

$$\Delta T = W\dot{Q} \ , \qquad (2.22)$$

where W is the thermal resistance of the sample and $\dot{Q}$ is the heating rate due to twisting the sample: $\dot{Q} = 0.05$ Watt. We assume that the sample end which is in touch with the central rod is at a constant temperature (10K). The thermal resistance of our K sample is about 38 K/Watt at 10K, and therefore the temperature drop $\Delta T \cong 2$K. Since we assumed that all the heat flowed the whole length of the sample, ΔT is an overestimate. In our experiment we have seen no noticeable temperature increase on our diode thermometer while smoothly deforming the sample.

2.9 Uncertainties

In our $(1/\rho)d\rho/dT$ measurements the biggest uncertainty below 0.15K comes from the determination of ΔC, whose uncertainty may exceed 10% at the lowest temperatures. Thus possible systematic uncertainties in ΔT are not significant below about 0.15K. For temperatures above 0.15K the uncertainty in ΔC is usually less than 2%. For $0.03K < T < 0.6K$, we

estimated in section 2.6 that the systematic uncertainty in T was less than 3%. If we restrict this estimate to T > 0.15K, we obtain 2%. Thus for T > 0.15K we estimate the uncertainty in $(1/\rho)d\rho/dT$ to be 3%. In converting $(1/\rho)d\rho/dT$ to $d\rho/dT$, we must include the uncertainty in ρ_o which we estimate to be ±3%.

In our G measurements the major source of uncertainty is from the thermal drifts of the system which cause the effective zero of the SQUID null detector to drift during the measurement of I_g. The uncertainty in I_g is less than 2% for temperatures above 0.1K, and it could be as large as 5 to 10% at the lowest temperatures (T< 0.05K), since thermoelectric voltage is usually very small in this temperature region. Other possible uncertainties are also negligible compared to those given above.

Chapter III Experimental Results

3.1 Resistivity

In our experiment two kinds of samples have been used: One is a pure potassium sample with Residual Resistance Ratio (RRR), which is defined as

$$RRR = R(293K)/R(4.2K), \tag{3.1}$$

and is of the order of 4100; and the other sample is a dilute K(Rb) alloy (K-0.087 at % Rb).

We used the K(Rb) sample so that the electron scattering rate would be dominated by a known impurity, Rb. For the most heavily deformed K(Rb) sample, we will see that this condition is still met since $\rho_d/\rho_i < 0.09$, where $\rho_o = \rho_d + \rho_i$. In this limit the theory of Kaveh and Wiser would predict a small increase in A with deformation. The presence of Rb impurities might also modify the dynamical properties of the dislocations.

3.1.1 Residual resistivity

From Eq.(1.11) we know the increase in ρ_o due to dislocations goes

linearly with the change in the dislocation density N_d:

$$\rho = WN_d. \qquad (1.11)$$

The coefficient W is predicted by Basinski (8) to be 4×10^{-19} Ωcm^3.

If we use the simple dislocation model shown in Fig. 1.2, we can obtain a linear relation between the dislocation density N_d and the twist angle θ (53)

$$N_d = 2\theta/bL \qquad (3.2)$$

where L is the sample length and b is the Burgers Vector.

From Eqs.(3.2) and (1.11), we see that the change in residual resistivity is predicted to vary linearly with the angle of twist. Fig. 3.1 is a plot of the change in ρ_o vs the twist angle θ for our K sample in a series of twists at 9.3K (open circles). It can be seen from the plot that a nice linear relation is obtained. As we will see later, about 70% of $\Delta\rho_o$ is due to vacancies, therefore one must assume that the vacancy concentration is also proportional to θ. The full circles are the data from van Vucht et al.(54). The data shown are corrected because their sample was 10 cm long and ours was 4 cm long. The higher slope of their data might be related to the higher yield stress of K at 4.2K. For our K-5 sample which was twisted 1329° at 9.3K, we have a change in ρ_o of $\Delta\rho_o \cong 0.7$ nΩcm. The corresponding change in $\Delta\rho_o$ due to the dislocations is estimated to be $\rho_d \cong 0.21$ nΩcm, which is the value

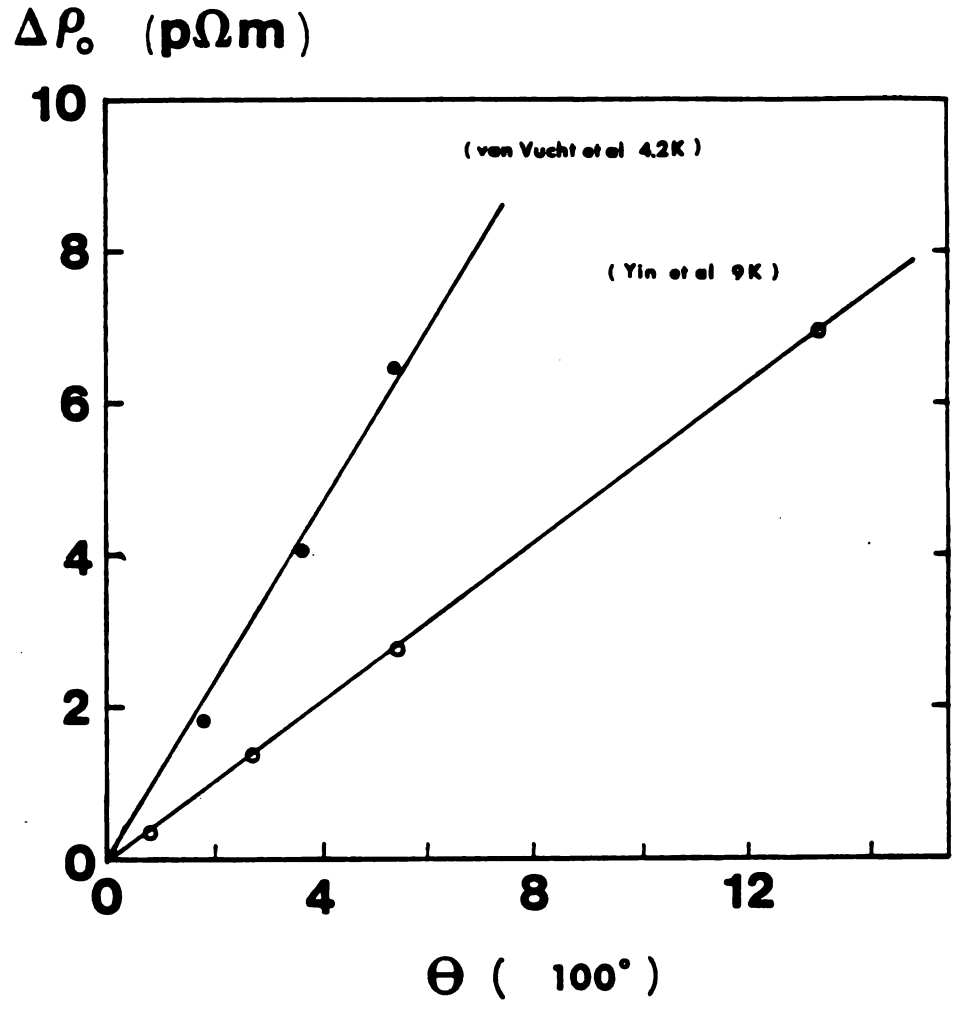

Figure 3.1
$\Delta\rho_o$ vs θ
$\Delta\rho_o$ is plotted as a function of the angle of twist for K samples (open circle). The full circles are the data from van Vucht et al.

of $\Delta\rho_o$ after the sample was annealed at 60K. With L~4cm, b~5Å for K, and θ = 1329° , Eqs.(3.2) and (1.11) predict that $\rho_d \sim 0.1$ nΩcm. Thus the theoretical and experimental values of ρ_d agree within a factor of 2.

We can also use (1.11) to estimate the dislocation density for our deformed sample. For our 1329° twisted sample K-5 with $\rho_d \cong 0.2$ nΩcm, Eq.(1.11) gives $N \sim 5 \times 10^9$ cm^{-2}.

3.1.2 K(Rb) data

In Fig. 3.2 we present a set of data obtained in a series of deformations. The theory of Kaveh and Wiser (19) would predict that the introduction of dislocations would only slightly increase the coefficient A of the e–e scattering T^2 term, since $\rho_d / \rho_i < 0.09$. Instead we see a rather different behavior for dρ/dT as we introduce dislocations. See Table 3.1 for details about the deformation procedures. Note that annealing at 200K very effectively removes the dislocations and essentially restores the behavior of dρ/dT to that seen before deformation.

We shall try to fit the data with

$$\rho(T) = AT^2 - C'T + (D/4T)\sinh^{-2}(E/2T), \qquad (3.3)$$

where AT^2 is the e–e effective scattering term and $-C'T$ is an anomalous term observed in our laboratory for unstrained alloy samples

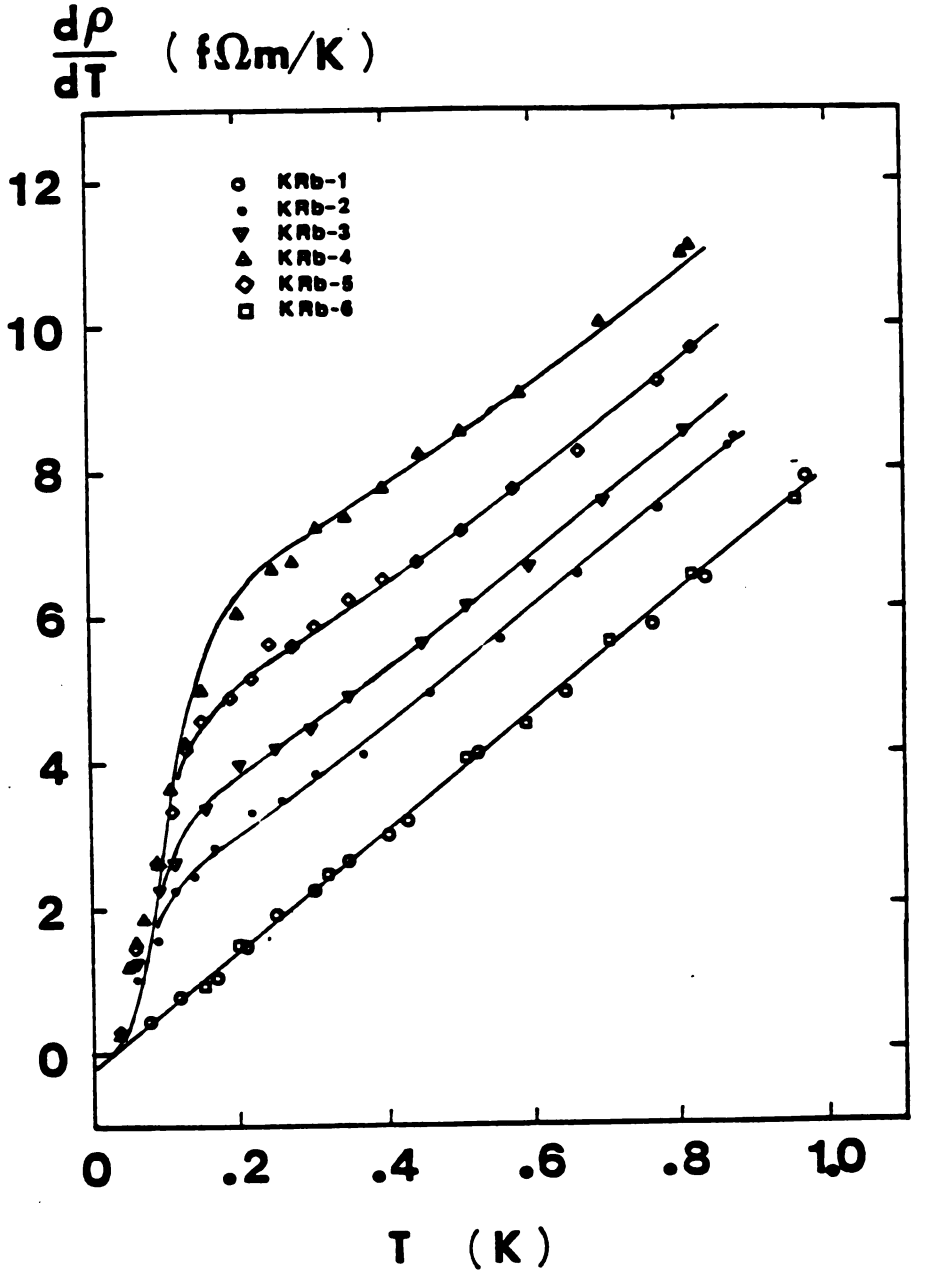

Figure 3.2
dρ/dT vs T for K(Rb) samples
dρ/dT is plotted as a function of T for the K(Rb) samples in a series of twists. The details are given in Table 3.1.

Table 3.1
K(0.087 at% Rb) Alloy Sample

Sample	$\rho_{4.2}$ (nΩcm)	ρ_o (nΩcm)	E_1(K)	D_1(fΩmK)	E_2(K)	D_2(fΩmK)
KRb-1	11.94	11.61	-	-	-	-
KRb-2	12.17	11.85	0.354±0.098	0.174±0.094	-	-
KRb-3	12.38	12.04	0.408±0.028	0.336±0.046	-	-
KRb-4	13.03	12.68	0.539±0.044	1.20±0.18	-	-
KRb-5	12.62	12.29	0.452±0.032	0.62±0.09	-	-
KRb-6	12.06	11.73	-	-	-	-
KRb-4	13.03	12.68	0.745±0.051	1.21±0.09	0.296±0.042	0.180±0.077

$A = 4.01 \pm 0.01$ (fΩm/K^2)

$C' = 0.22 \pm 0.01$ (fΩm/K)

The temperature is limited to T < 0.7K in the least-squares fit.

KRb-1 Untwisted

KRb-2 480° twisted at 60K

KRb-3 4800° twisted (total) at 60K

KRb-4 additional 4800° at 9.3K then annealed at 36K for 30 min.

KRb-5 annealed at 60K for 30 min.

KRb-6 annealed at 200K for 2 hrs.

with high concentration of impurities(55), which is not of interest to this work. The third term is the vibrating dislocation term modeled by Gantmakher and Kulesco (Eq. 1.27), which was also used by M. Haerle et al. in their work. The coefficients A and C′ were obtained from the fit of the undeformed sample KRb-1 and were then kept constant in the fits of the deformed samples KRb-2 to KRb-5 where the vibrating dislocation term (1.27) was introduced.

Table 3.1 also shows how the various parameters change as the deformation is increased.

In Fig. 3.2 we obtain reasonably good fits with the vibrating dislocation model. For sample KRb-4 we see a significant deviation below 0.2K. This fit can be improved by assuming that there is more than one frequency in the spectrum of the vibrating dislocations. Fig. 3.3 shows such an improved fit. In this figure we plotted $d\rho/dT - (2AT-C')$ vs the temperature. In this way we see more clearly the step-like function in $d\rho/dT$ caused by deforming the samples. The dotted lines are the fits plotted in Fig. 3.2, and the solid curve is the fit using a two-frquency model

$$\rho(T) = AT^2 - C'T + (D_1/4T)\sinh^{-2}(E_1/2T) + (D_2/4T)\sinh^{-2}(E_2/2T) \quad . \quad (3.4)$$

The parameters of this two frequency fit for KRb-4 are also given in Table 3.1.

Our success in making $d\rho/dT$ measurements well below 80 mK was necessary in order to establish the need for this two-frequency fit. We

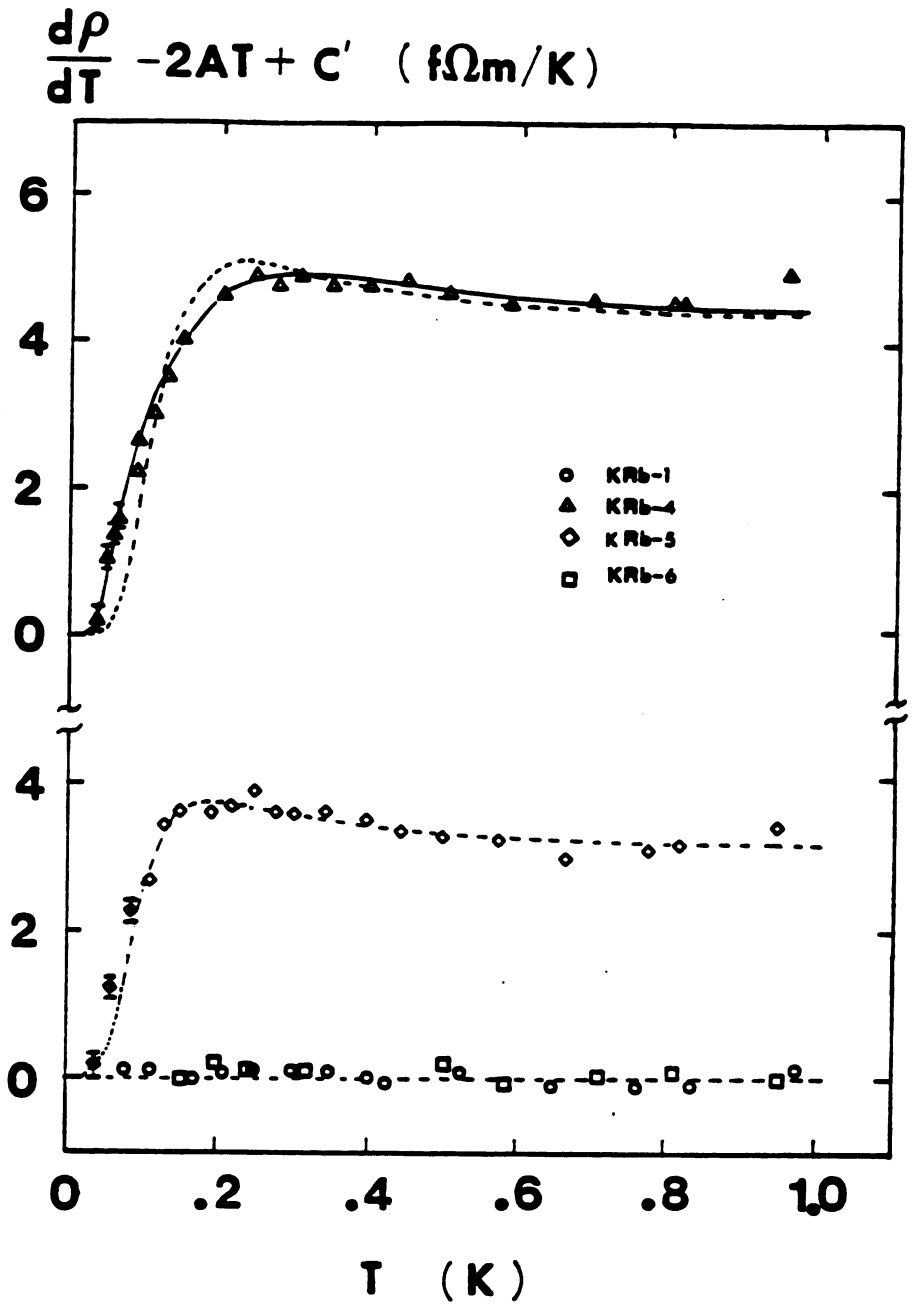

Figure 3.3
dρ/dT - (2AT-C´) vs T for K(Rb) samples
dρ/dT - (2AT-C´) is plotted as a function of T for the K(Rb) samples. A step-like function is seen for samples KRb-4 and KRb-5.

recall that making measurements down to about 20 mK was one of the goals of this research.

It is worth mentioning here that the one-frequency model seems to be adequate for samples KRb-2, KRb-3 and KRb-5, which are deformed at 60K or annealed at 60K after deformation at 9.3K. From Chapter I we know that the all vacancies in potassium will not be annealed out until 60K. Since KRb-4 was annealed only at 36K, we might ascribe this multi-frequency behavior to the presence of vacancies in the sample.

From Table 3.1 we see a saturation in the residual resistivity when twisting at 60K. For KRb-2 we twisted 480°, and we got an increase in ρ_o of about 0.23 nΩcm. In KRb-3 we twisted about 10 times more, but the change in ρ_o is only 0.44 nΩcm. We may ascribe this to the following fact: After the sample has been twisted back and forth several times, there will exist dislocations with opposite-sign Burgers vectors which can annihilate if they are close enough. The dislocation density will then saturate when the annihilation and generation rates are equal.

3.1.3 Pure K data without annealing

To see the effect of small angle twists, we did a series of deformations in a pure K sample with RRR ~ 4100. We saw behaviors which were similar to the K(Rb) samples. The magnitude of the step-like function went up systematically as the amount of deformation was increased. Recall that Fig. 3.1 shows that ρ_o increases linearly with

the total angle of twist for this sample. In Figs. 3.4 and 3.5 and in Table 3.2 we show the data and parameters obtained in a least-squares computer fit.

We first fit K-1 by using

$$\rho(T) = AT^2 \qquad (3.5)$$

to obtain the value of A. We then kept A constant in the fits of the strained samples. For K-2, K-3, K-4 and K-5 we used

$$\rho(T) = AT^2 + (D_1/4T)\sinh^{-2}(E_1/2T) \qquad (3.6)$$

with T < 0.6K so that the electron-phonon scattering terms were negligible. In Fig. 3.4 we plot $(\rho_{4.2}/\rho)d\rho/dT$ vs T and see a reasonably good fit. Fig. 3.5 shows the plot of $(\rho_{4.2}/\rho)d\rho/dT - 2A'T$ where the step-like behavior is clearer. Since $(\rho_{4.2}/\rho)d\rho/dT$ is what we actually measure during the experiment, we fit our equations to this form of the data; and A' which appears in Figs. 3.5 and 3.6 is a parameter related to A by: $A = (\rho_o/\rho_{4.2})A'$. Typically $\rho_{4.2}$ is 15% larger than ρ_o, which we define to be ρ at about 30mK. All the parameters in the tables have been properly corrected. Since $\rho_{4.2}$ is very close to ρ_o for the K(Rb) sample, we chose to convert that data directly to $d\rho/dT$.

We see a rapid increase in Figs. 3.4 and 3.5 for T > 0.6K, and this has been ascribed to the quenching of phonon drag, which results in the reappearance of the normal electron-phonon scattering term CT^5.

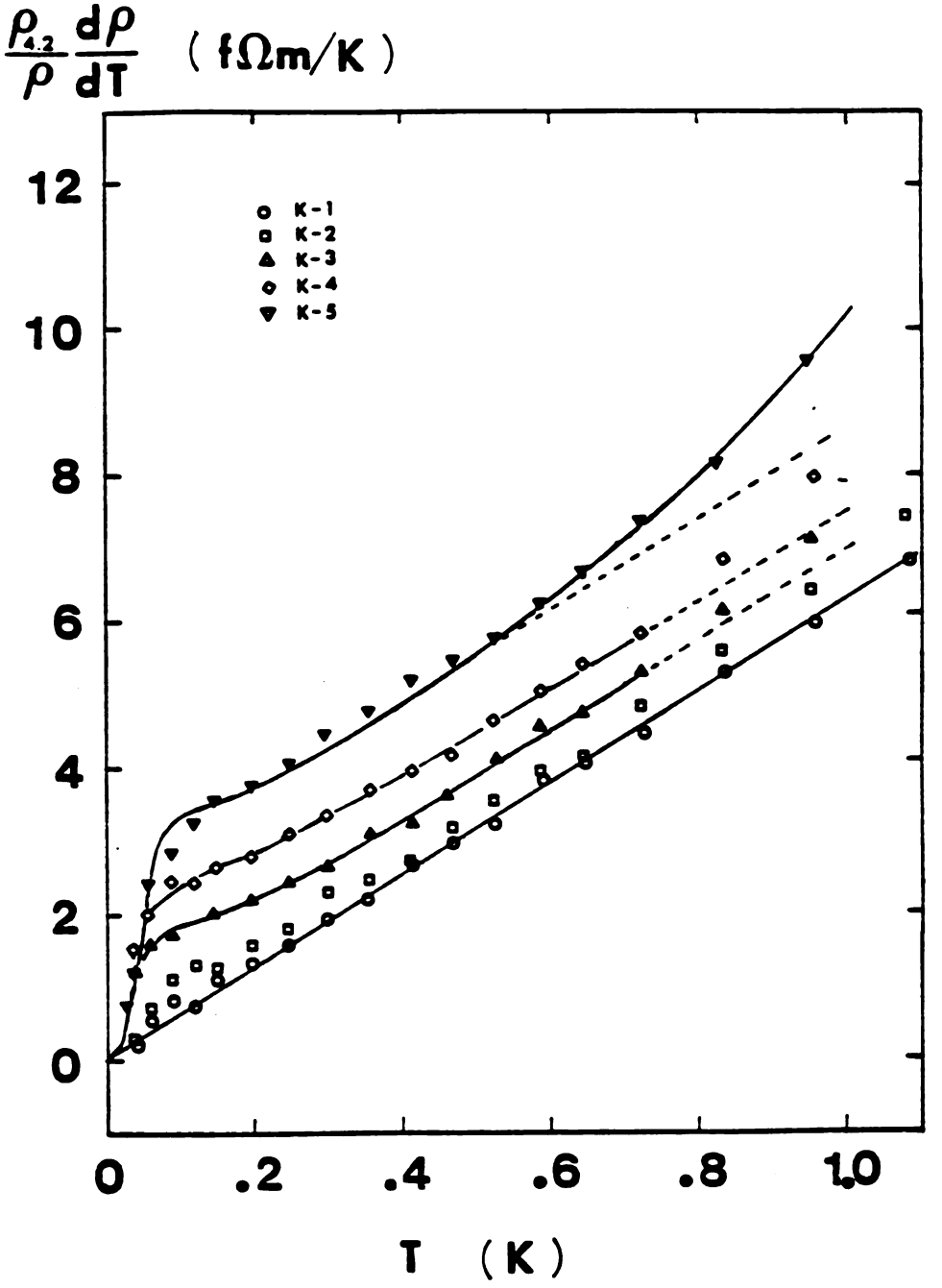

Figure 3.4
$(\rho_{4.2}/\rho)d\rho/dT$ vs T for the pure K samples.
The samples are twisted at 9.3K without annealing. The details of twist are given in Table 3.2.

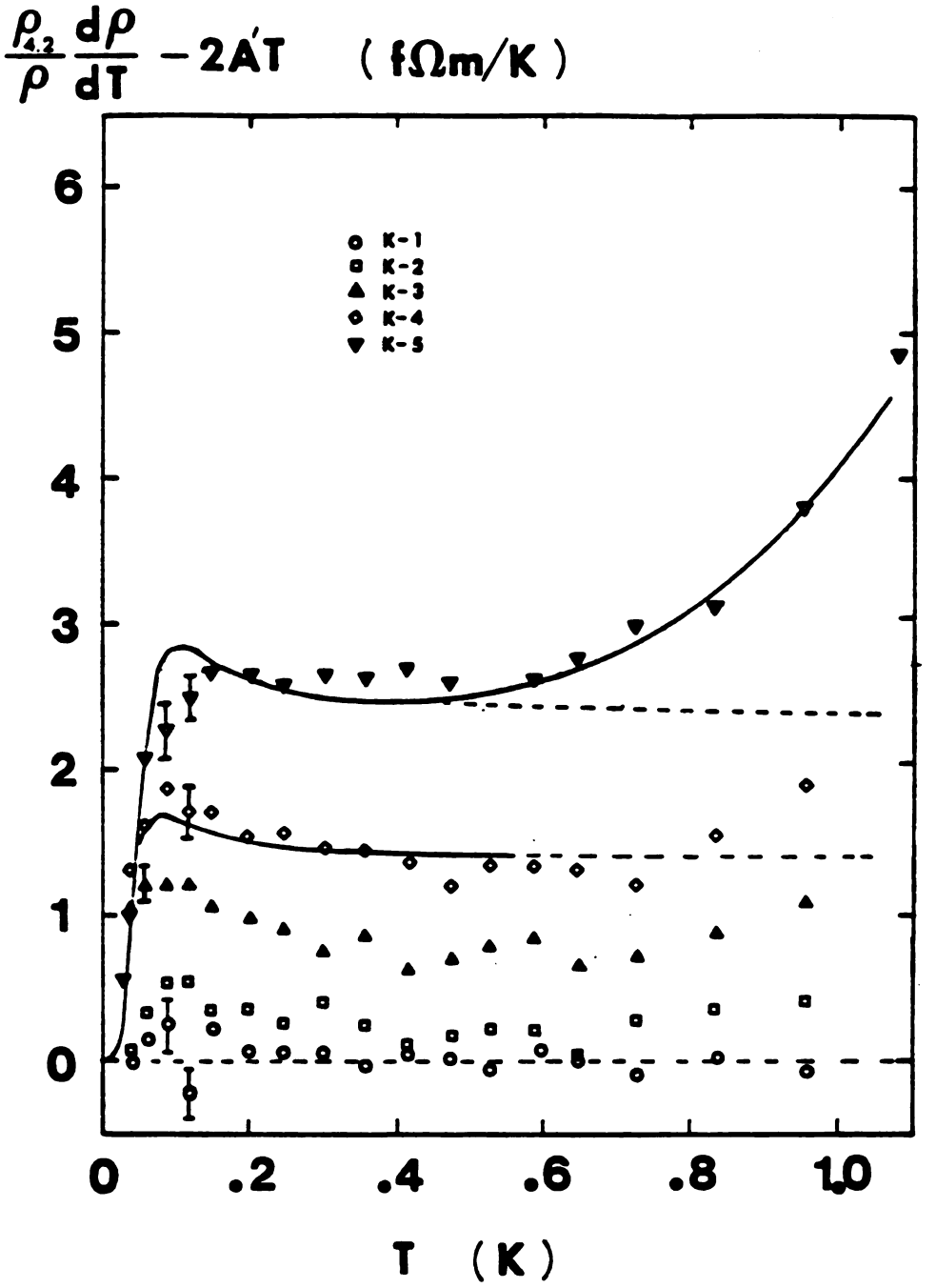

Figure 3.5
$(\rho_{4.2}/\rho)d\rho/dT - 2A'T$ vs T for the unannealed K samples
A step-like function is seen. The solid and dashed curves are the best computer fits. Details are given in the text.

Table 3.2
Pure K Sample Without Annealing

Sample	ρ_{42} (nΩcm)	ρ_o (nΩcm)	E_1(K)	D_1(fΩmK)	E_2(K)	D_2(fΩmK)
K-1	1.776	1.497	-	-	-	-
K-2	1.805	1.531	0.219±0.080	0.012±0.009	-	-
K-3	1.908	1.632	0.152±0.046	0.019±0.011	-	-
K-4	2.056	1.773	0.179±0.023	0.041±0.010	-	-
K-5	2.489	2.193	0.242±0.036	0.124±0.036	-	-
K-5	2.489	2.193	0.162±0.014	0.041±0.009	0.580±0.050	0.210±0.023

$A = 2.66 \pm 0.02$ (fΩm/K^2)

$C = 0.300$ (fΩm/K)

K-1 untwisted

K-2 77° at 9.3K

K-3 267° at 9.3K

K-4 540° at 9.3K

K-5 1329° at 9.3K

The solid curve for K-5 shows the improved fit with a CT^5 term added to Eq.(3.6). From the Table 3.2 we see that the value of C is less than 0.35 $f\Omega m/K^5$, the theoretical value predicted by Frobose (56) for totally quenched phonon drag.

As we did with KRb-4, we can also improve the low temperature fit for T < 0.6K by using a two frequency model

$$\rho(T) = AT^2 + (D_1/4T)\sinh^{-2}(E_1/2T) + (D_2/4T)\sinh^{-2}(E_2/2T) \qquad (3.7)$$

Fig. 3.6 shows such a plot. We fit Eq.(3.7) only to K-5 because the improvement there was significant. The parameters are also given in Table 3.2.

In Fig. 3.7 we plot the parameter D in Eq.(3.6) as a function of $\Delta\rho_0$ for both K(Rb) and K samples. The circles are the data from the K sample which was twisted at 9.3K without annealing, and the triangles are the data from the K(Rb) samples. We see in the plot that deformation systematically increased D for both K(Rb) and K samples. Indeed D varies almost linearly with $\Delta\rho_0$ which is in agreement with our expectation that $D \sim N_d$. For a comparison, we also plot Haerle's data in the figure: the diamond is from his K(Rb) sample KRbhb, which was deformed at 60K; and the square is from his K sample Kh9b, which was deformed at 4.2K. We see that they are in agreement with our data points even though a rather different method of deformation was used. It should be pointed out here that the K(Rb) samples were deformed or annealed at 60K, where the vacancies are believed to anneal out.

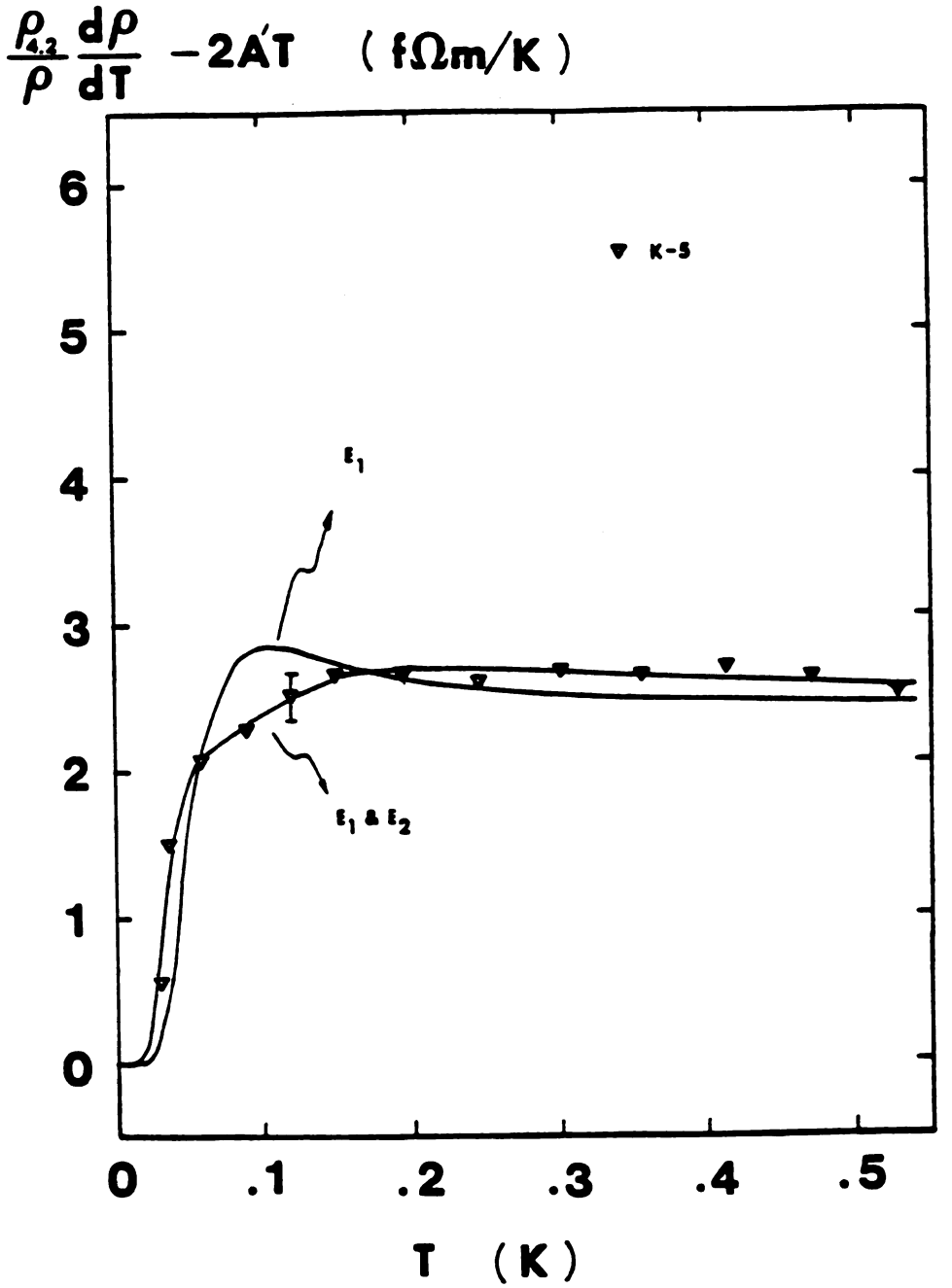

Figure 3.6
A two-frequency fit vs the one frequency-fit for sample K-5.
An improved fit is obtained.

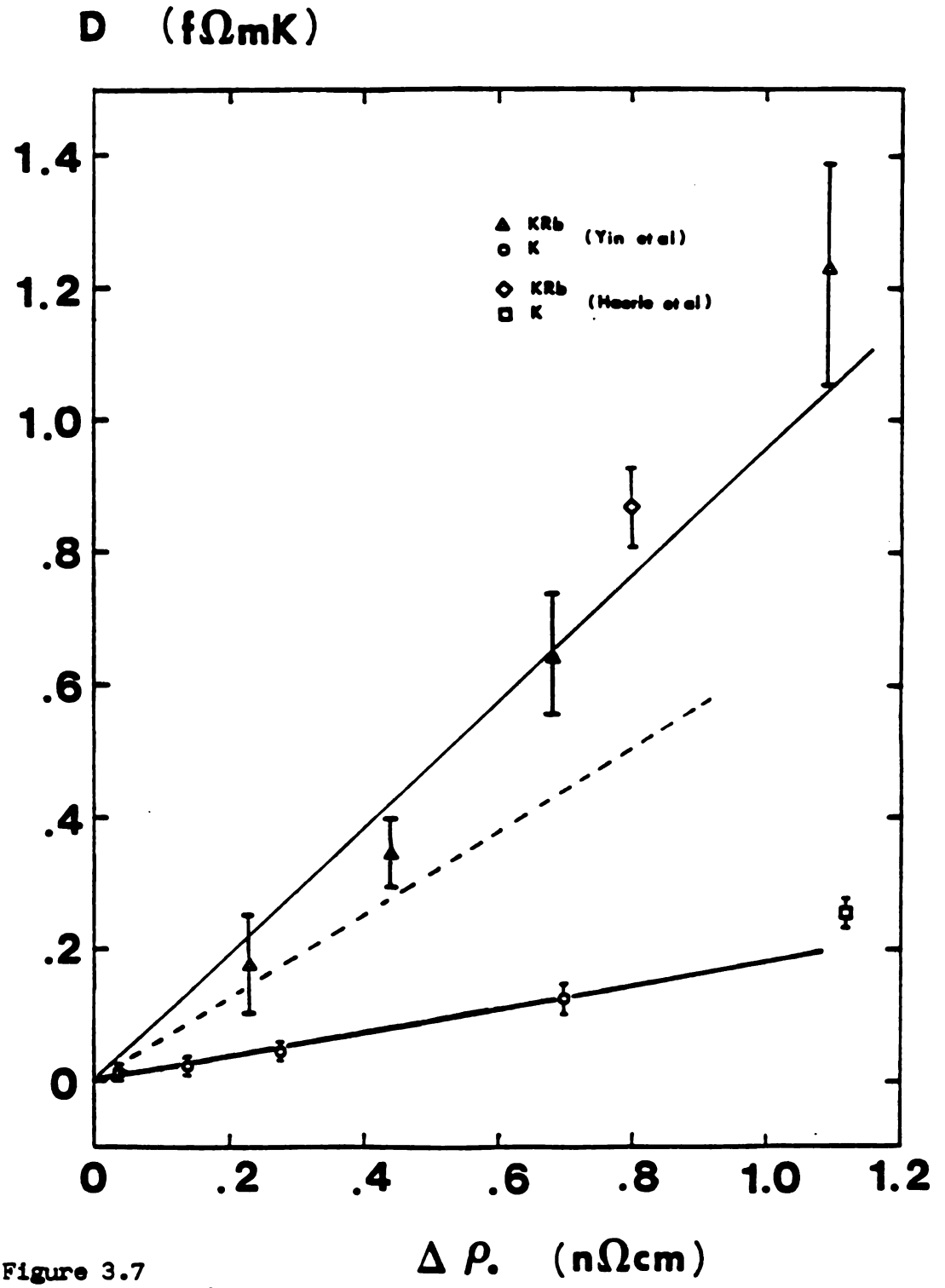

Figure 3.7
D vs $\Delta\rho_o$ for K(Rb) and K samples
The coefficient D of Eq.(3.3) or Eq.(3.6) is plotted as a function of $\Delta\rho_o$ for the K(Rb) samples or pure K samples with out annealing. The data from Haerle et al. are also shown. The dashed line is the fit to the K samples after the vacancy contribution is corrected for, see text for details.

However, the K samples were deformed at 9.3K, where vacancies, as well as screw dislocations, were produced. From Tables 3.2 and 3.3 below we see that for our sample K-5, which was deformed at 9.3K, $\Delta\rho_o$ = 0.696 nΩ cm, and for K-7, which was annealed at 60K, $\Delta\rho_o$ = 0.207 nΩcm. We see that 70% of the increase in $\Delta\rho_o$ with deformation at 9.3K is due to vacancies. If we correct for this and plot D vs ρ_d (due to dislocation contribution only), we get the dotted line in the figure.

We see from the plot that the K(Rb) data have a slope higher than that of the K sample. We know for a bcc metal that at 9K, deformation produces more screw dislocations than edge dislocations, and at 60K, deforming K is thought to produce more edge dislocations(6). Perhaps the difference in the slopes is due to the different dislocations in these K(Rb) and K samples or to the presence of Rb in one of them.

For the vibrating dislocation mechanism, we have discussed two possible models in Chapter I. One is the Granato model (37) in which the dislocation is considered to be a vibrating elastic band stretched between two pinning points. The resonant frequency is given by

$$\nu = V/3L \qquad (1.25)$$

where V is the transverse phonon velocity and L is the pinned dislocation length. From Eq.(1.11) we know that ρ_d is proportional to the dislocation density N_d; and if we simply assume $N_d \cong 1/L^2$, then

$$\nu \sim (\rho_d)^{\frac{1}{2}} \qquad (3.8)$$

Thus the characteristic frequency (or energy) is proportional to the square root of ρ_d . The other model is associated with the Peierls potential in which the dislocation oscillates. The characterestic frequency is given in Chapter I as

$$\nu = (\tau_p/4\pi^2\rho_m b)^{\frac{1}{2}} \qquad (1.26)$$

where τ_p is the Peierls stress, ρ_m is the mass density and b is the Burgers vector. An important feature of this model is that the vibration frequency is independent of the dislocation segment length L and consequently, is independent of ρ_d.

In Fig. 3.8 we plot the characteristic energy E, obtained by fitting Eq. (3.3) or (3.6) to the K(Rb) data and the unannealed K data as a function of $\Delta\rho_o$. We also plot the data from Haerle et al. in the figure, and we see that they are also in agreement with our data. For our K(Rb) data, there seems to be a systematic increase in E with $\Delta\rho_o$, which might imply that the Granato model is applicable. Unfortunately, the error bars are sufficiently large that we cannot discriminate between $E \sim \Delta\rho_o$ and $E \sim (\Delta\rho_o)^{\frac{1}{2}}$. For our K samples: we do not see a really significant $\Delta\rho_o$ dependence in E.

3.1.4 Pure K data after annealing

When we anneal the K(Rb) samples at 60K, we see a drop in the

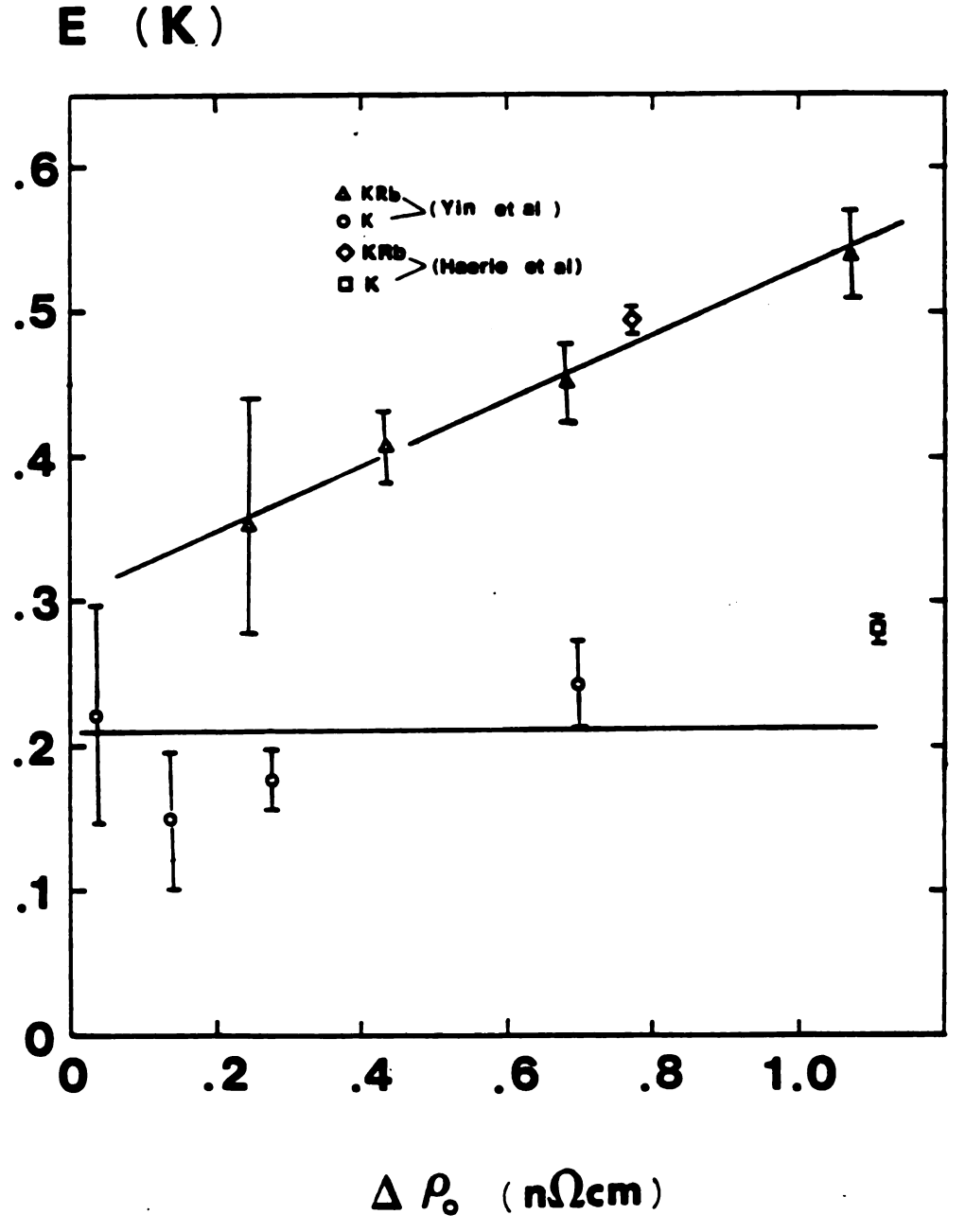

Figure 3.8
E vs $\Delta\rho_o$ for K(Rb) and K samples
The characteristic energy E is plotted as a function of $\Delta\rho_o$ for the K(Rb) and K samples. The data from Haerle et al. are in agreement with ours.

height of the step-like function in $d\rho/dT$ (Fig. 3.3). However, when we anneal the K samples at 60K, we see a peak rising even above the height of the step of the unannealed samples. This is shown in Fig 3.9 in which we again plotted $(\rho_{4.2}/\rho)d\rho/dT-2A'T$ as a function of T. The dashed curve is the best fit to K-5, which was twisted at 9.3K without annealing. The solid curves are the fits to the data which we will discuss below.

To fit this peak we tried several models. The vibrating dislocation model Eq.(3.6) failed to fit this peak, even with two frequencies. Then we tried to let A be a variable parameter in Eq.(3.6). In Table 3.3 we present the fitting parameters obtained by using this method. Figure 3.10 is such a plot in which we show the fit to K-7(solid curve). The parameter A' in Fig. 3.10 is from Table 3.2 and is derived from $A=2.66\ f\Omega m/K^2$. Since A in Table 3.3 is smaller than $2.66\ f\Omega m/K^2$, the fit in Fig. 3.10 has a negative slope at higher temperatures. The fit was done for $T < 0.55K$ where the phonon contribution is negligible. To fit the data for $T > 0.6K$, a CT^5 term has to be added where C was found to be $0.30\ f\Omega m/K^5$, which is less than the maximum value $0.35\ f\Omega m/K^5$ predicted by Frobose(56). We had an improved fit. However, the resulting drop in A turned out to be hard to explain since the theory of Kaveh and Wiser (19) predicted that the introduction of dislocation would only increase A.

To avoid letting A become smaller, we then tried the following method: we thought that the peak might be associated with some other mechanism and used the following:

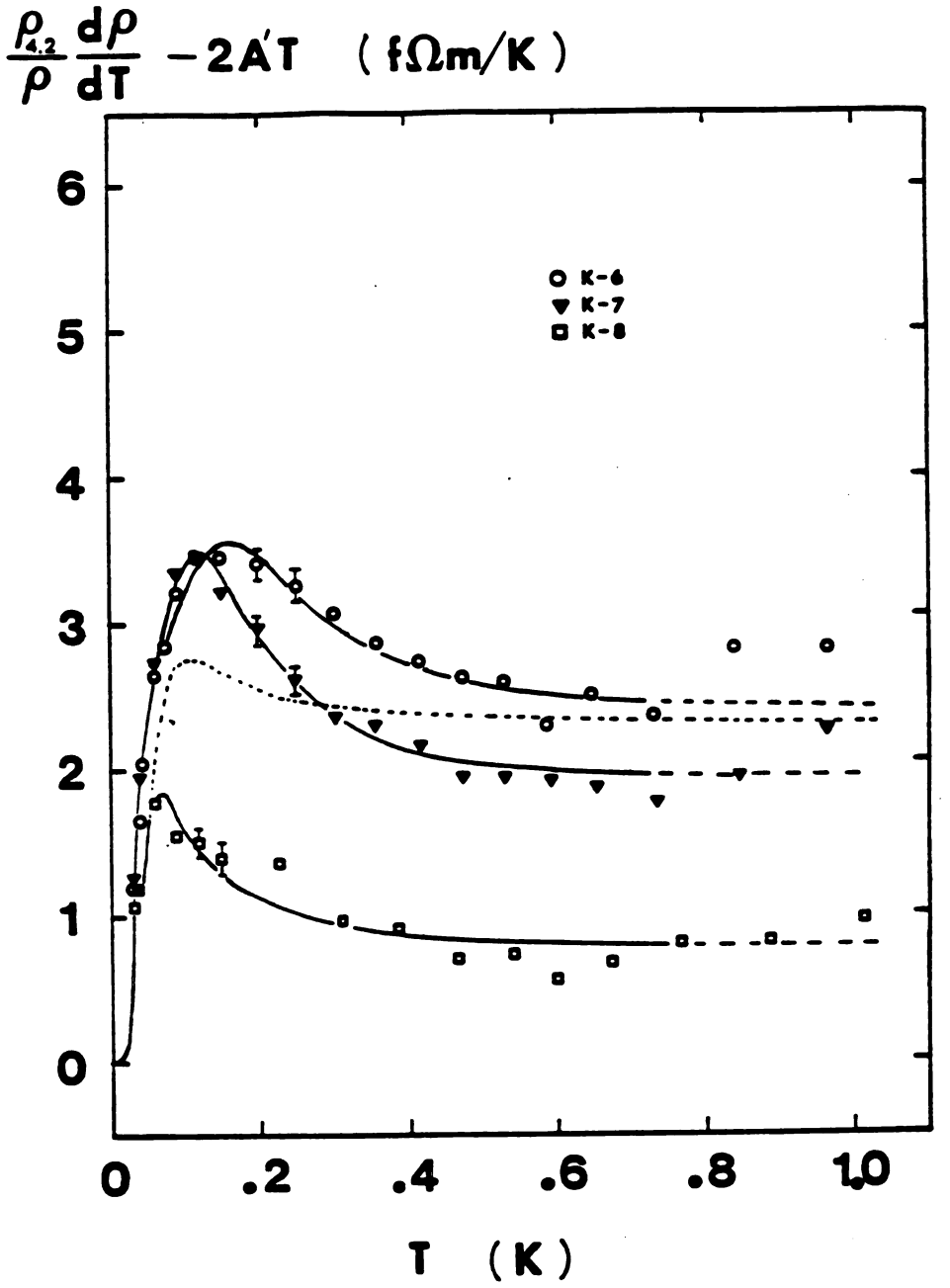

Figure 3.9
$(\rho_{4.2}/\rho)d\rho/dT - 2A'T$ vs T for the annealed pure K samples
A peak is seen at 0.2K. The dashed curve is the best fit for the unannealed sample K-5. The solid curves are explained in the text.

Table 3.3
Pure K sample with A as a variable parameter

Sample	$\rho_{4.2}$ (nΩcm)	ρ_0 (nΩcm)	A (fΩm/K^2)	E (K)	D (fΩmK)
K-1	1.776	1.497	2.655±0.018	-	-
K-2	1.805	1.531	2.422±0.073	0.242±0.046	0.022±0.009
K-3	1.908	1.632	2.319±0.066	0.156±0.023	0.023±0.006
K-4	2.056	1.773	2.441±0.062	0.183±0.016	0.046±0.008
K-5	2.489	2.193	3.167±0.129	0.218±0.025	0.089±0.020
K-6	2.095	1.806	2.289±0.137	0.254±0.020	0.174±0.028
K-7	1.985	1.704	1.638±0.088	0.222±0.018	0.132±0.021
K-8	1.853	1.574	1.959±0.074	0.143±0.020	0.027±0.008

The temperature range is limited to T < 0.55K

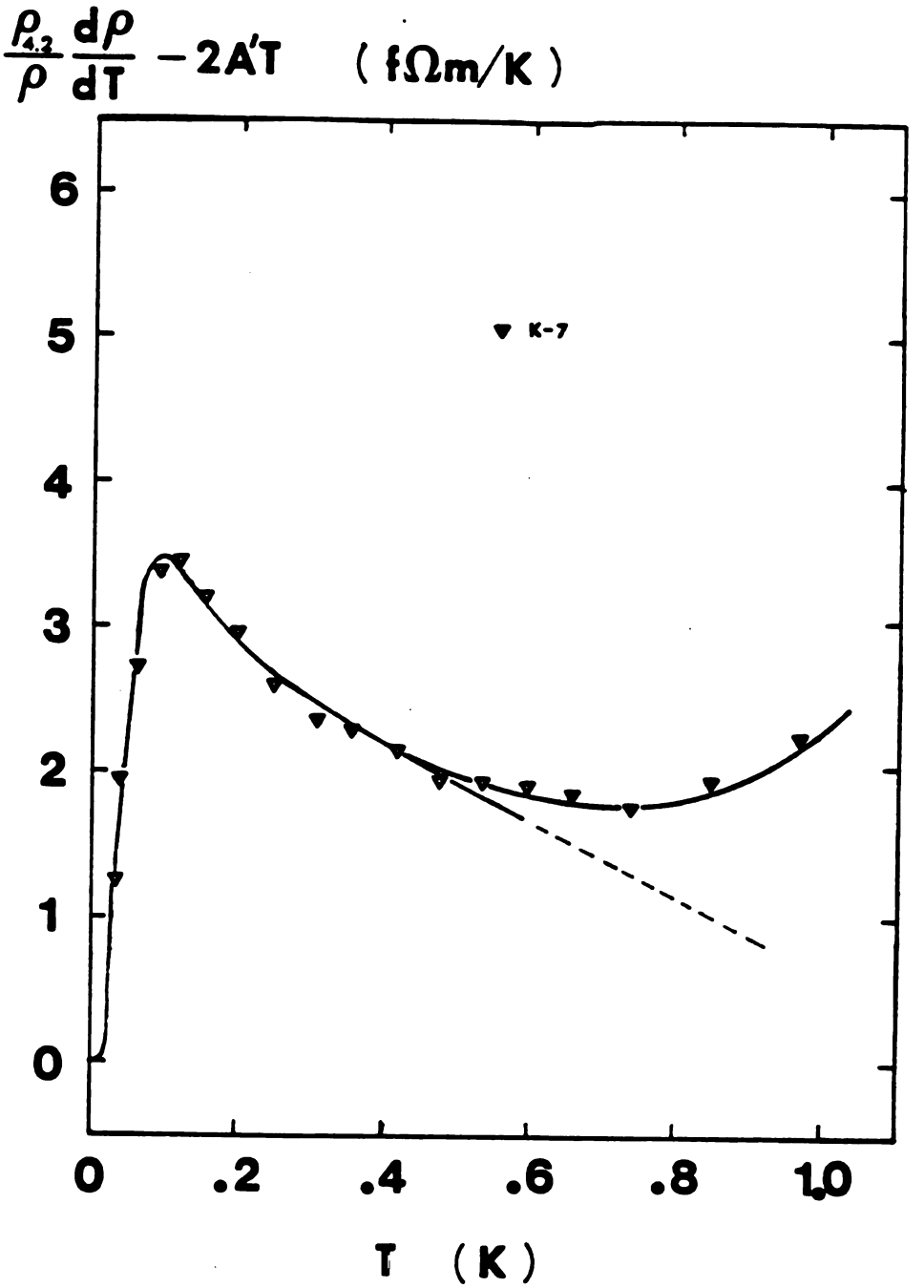

Figure 3.10
The improved fit to K-7 with A as a variable parameter
The dashed curve is without the CT^5 term. A CT^5 term helps to fit the rising tail of the data.

Table 3.4
Pure K samples after annealing or deformation at 60K
(The parameters are for Eq. (3.10).)

Sample	$\rho_{4.2}$ (nΩcm)	ρ_o (nΩcm)	E_1 (K)	D (fΩmK)	E_2 (K)	B (fΩm)
K-6	2.095	1.806	0.184±0.014	0.072±0.012	0.530±0.020	0.222±0.025
K-7	1.985	1.704	0.140±0.017	0.033±0.009	0.372±0.013	0.227±0.015
K-8	1.853	1.574	0.51±0.36	0.18±0.23	0.182±0.052	0.145±0.079
K2-1	1.622	1.380	-	-	-	-
K2-2	1.879	1.618	0.172±0.021	0.053±0.013	0.430±0.016	0.240±0.019

$A = 2.66 \pm 0.02$ (fΩm/K^2)

K-6 annealed at 35K for 30 min.

K-7 annealed at 60K for 30 min.

K-8 annealed at 100K for 30 min.

$A = 2.43 \pm 0.02$ (fΩm/K^2)

K2-1 untwisted

K2-2 2510° at 60K

$$\rho(T) = AT^2 + (D/4T)\sinh^{-2}(E_1/2T) + a(1+b\exp(E_2/T))^{-1} \qquad (3.9)$$

where the last term is the model of the localized electronic levels associated with dislocations, also proposed by Gantmakher and Kulesco [Eq.(1.23)]. With A still fixed, we had a very good fit; unfortunately, the parameters a and b were so strongly correlated with each other that we could not obtain any sensible values for them.

We finally used the following formula which gave us a curve that was almost identical to that for Eq.(3.9):

$$\rho(T) = AT^2 + (D/4T)\sinh^{-2}(E_1/2T) + B[1 + (2/3)\sinh^2(E_2/2T)]^{-1} \qquad (3.10)$$

where the third term, proposed by Fulde and Peschel(35), is due to inelastic scattering off localized energy levels produced by a crystalline electric field. The advantage of using Eq.(3.10) instead Eq.(3.9) is that the parameter B was well-behaved in the computer fit, which made it easier to analyse the data.

In Fig. 3.9 the solid curves show the fits using Eq.(3.10). We limit the temperature range to $T < 0.6K$ where the phonon terms are negligible. The parameters from the least-squares fit using Eq.(3.10) are given in Table 3.4. We see that the new term in Eq.(3.10) has been used to fit primarily the prominent peak in the annealed K data. No such term is needed for the annealed K(Rb) data.

3.1.5 Annealing at 60K after deformation at 9.3K vs deforming directly at 60K for K samples.

If the peak arising in $d\rho/dT-2A'T$ for K after annealing (Fig. 3.9) is due to some complicated process which occurred during annealing, then the question arises as to whether the peak will still be there if we directly deform our K sample at 60K. In Fig. 3.11 we make such a comparison. K-7 is the sample which was twisted by 1329° at 9.3K and then annealed at 60K. K2-2 is another K sample which was twisted by 2510° at 60K. The fitting parameters for these samples are given in Table 3.4. In Fig. 3.11 we see that these two samples have remarkably similar behaviors which correlate well with their similar values of $\Delta\rho_o$ where $\Delta\rho_o$ = 0.21 nΩcm and 0.24 nΩcm for K-7 and K2-2, respectively. Note that K2-2 required a much larger angle of twist at 60K. Thus the electron scattering characteristics of the dislocations seem to depend only on the fact that the sample was heated to 60K and not on the process of deformation and annealing.

3.1.6 Comparison of 60K annealed pure K sample with those of Haerle et al.

In Figs. 3.7 and 3.8 our values of D and E were in good areement with those of Haerle et al. We wish now to compare our results presented in Fig. 3.9 - 3.11 with theirs. Since Haerle et al. were able to fit their data for samples deformed at 60K with a single-energy

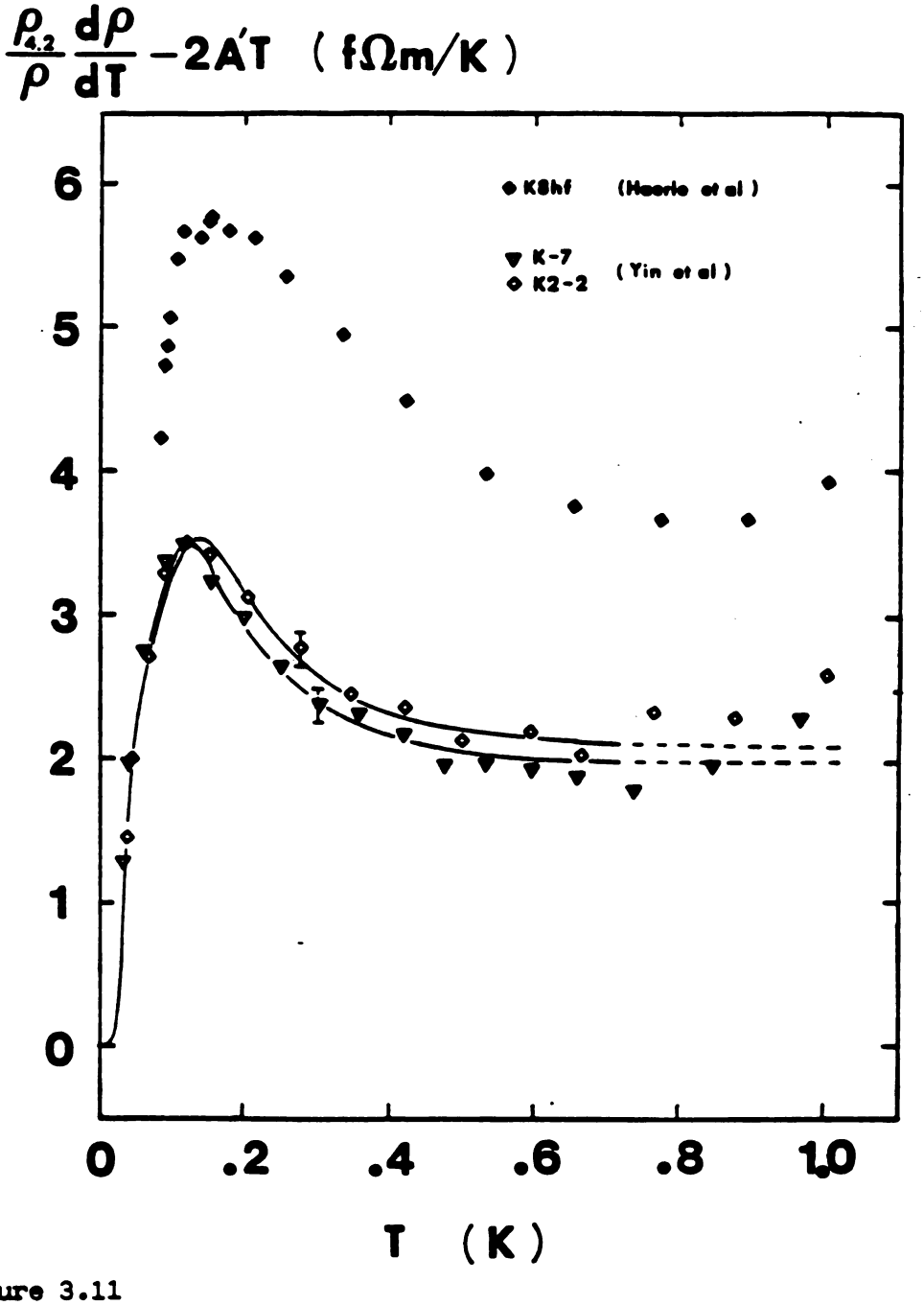

Figure 3.11
A comparison between annealing at 60K after twisting at 9.3K (K-7) and twisting directly at 60K (K2-2)
A similar behavior is seen. The data of Haerle et al. are also presented.

vibrating dislocation model [Eq.(3.6)], there would seem to be a contradiction between our respective results. We now believe that this disagreement is not real and that the "size-effect" contribution to their undeformed 0.9-mm-diameter samples was probably not corrected for properly in their deformed samples. In undeformed samples this size effect shows up as an apparent e-e term in ρ of the form: T^n where $n<2$. If their very lowest temperature data were constrained to fit a T^2 behavior, then they obtained $A = 1.5\ f\Omega m/K^2$ which is much smaller than typical values of A ($2.5\ f\Omega m/K^2$) for our 2-mm-diameter samples. It is not known what happens to the size effect contribution when the sample is deformed. Haerle et al. fit Eq.(3.6) to their data and obtained $1.0 \lesssim A \lesssim 1.5\ f\Omega m/K^2$ for their deformed samples. Since the A's before and after deformation were comparable, it was implicitly assumed by Haerle et al. that the size effect was not significantly changed by deformation. If, on the contrary, we assume that severe deformation eliminated the size effect in the data of Haerle et al. and raised A to about $2.5\ f\Omega m/K^2$, then their results look very much like ours. In Fig. 3.11 we present their data for sample K8hf which was severely deformed at 60K with $\Delta\rho_o = 0.73\ n\Omega cm$ where $A = 2.5\ f\Omega m/K^2$ rather than their value of $1.34 \pm 0.07\ f\Omega m/K^2$. Plotted in this way, their data behave in a very similar manner to ours. To uncover this unusual behavior in our 60K annealed sample, 2-mm-diameter samples were necessary so that this size effect was eliminated.

3.2 Thermoelectric ratio

From Chapter I we know that the thermoelectric ratio G for potassium below 1K is expected to obey

$$G = G_0 + bT^2, \qquad (1.40)$$

where G_0 is the diffusion term and bT^2 is the normal phonon drag term.

In Figs. 3.12 and 3.13 we present the G data for the K(Rb) and K samples. We can fit K-1 and KRb-1 reasonably well(solid curves) by using Eq.(1.40), but we see the fit is not as good for the strained samples (the dashed curves). For most of the strained samples, there is a maximum in G at about 0.5K. We then tried the following empirical formula

$$G = G_0 + aT + bT^2 , \qquad (3.11)$$

and we obtained much improved fits. The solid curves except K-1 and KRb-1 show these fits. The reason for the down-turn at the lowest temperatures, below 0.1K, is not known at this time.

The parameters obtained from the least-squares fit are given in Table 3.5. It is clear that dislocations make a negative contribution to G_0 in a systematic way.

In Chapter I we have shown the Gorter-Nordheim relation for

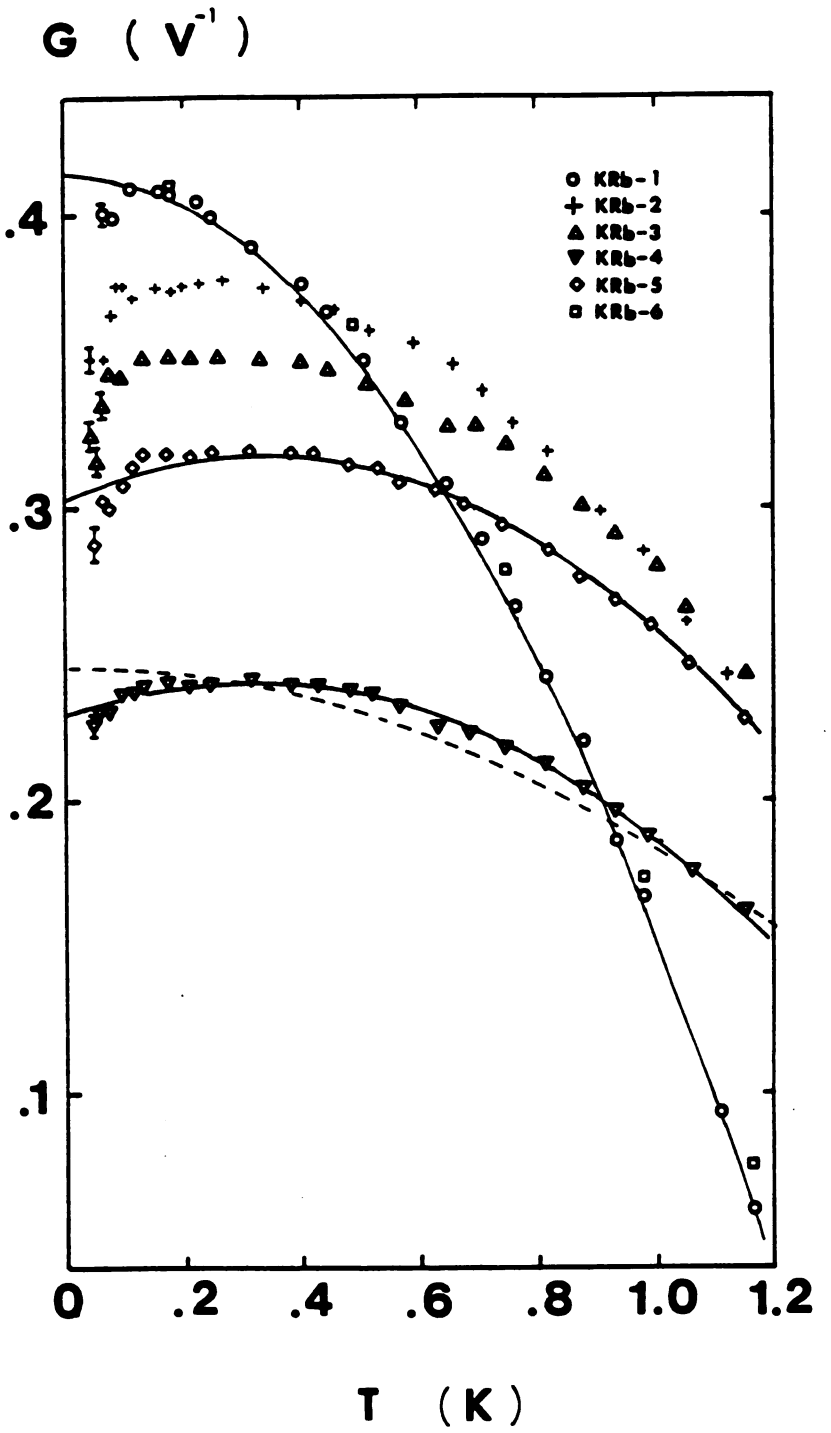

Figure 3.12
G vs T for the K(Rb) samples
Details of the fit are given in the text.

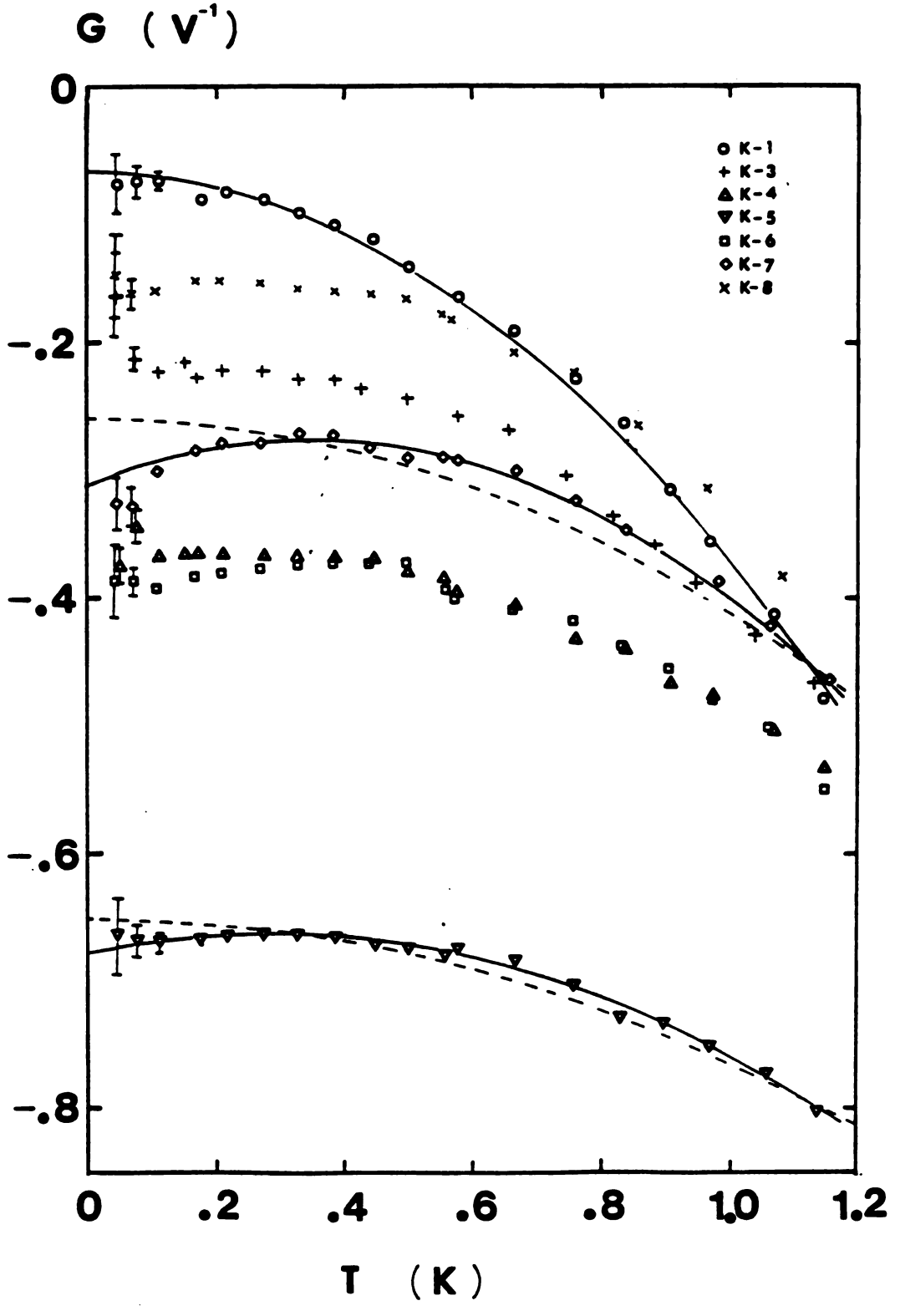

Figure 3.13
G vs T for the pure K samples.

Table 3.5
Parameters in G for the K(Rb) and K samples

Sample	ρ_o (nΩcm)	G_o(1/V)	a (1/VK)	b ($1/VK^2$)
KRb-1	11.61	0.415±0.001	-	-0.260±0.003
KRb-2	11.85	0.362±0.002	0.099±0.008	-0.185±0.006
KRb-3	12.04	0.337±0.002	0.093±0.010	-0.153±0.008
KRb-4	12.68	0.230±0.001	0.072±0.004	-0.115±0.003
KRb-5	12.29	0.303±0.002	0.092±0.005	-0.138±0.003
KRb-6	11.73	0.420±0.002	-	-0.256±0.003
K-1	1.497	-0.065±0.003	-	-0.303±0.004
K-2	1.531	-0.119±0.004	0.124±0.014	-0.358±0.010
K-3	1.632	-0.230±0.006	0.118±0.023	-0.296±0.018
K-4	1.773	-0.369±0.003	0.063±0.013	-0.178±0.010
K-5	2.193	-0.677±0.003	0.105±0.009	-0.187±0.006
K-6	1.806	-0.408±0.004	0.193±0.015	-0.276±0.011
K-7	1.704	-0.312±0.004	0.204±0.015	-0.292±0.011
K-8	1.574	-0.175±0.004	0.177±0.012	-0.334±0.009

G_d(KRb) = -1.78±0.19 (1/V)

G_d(K) = -1.967±0.014 (1/V)

diffusion thermopower:

$$S = S_d + (\rho_i/\rho)[S_i - S_d] \qquad (1.32)$$

where S_i and S_d are the diffusion thermopowers due to impurity scattering and dislocation scattering, respectively. We know that the thermopower S can be related to the thermoelectric ratio G by

$$G = S/LT \qquad (1.38)$$

where L is the Lorenz ratio which is approximately a constant below 1K. Therefore we have

$$G_e = G_d + (\rho_i/\rho)[G_i - G_d] \ , \qquad (3.12)$$

where G_d and G_i correspond to the diffusion thermoelectric ratio due to dislocation scattering and impurity scattering, respectively. If we plot G_e as a function of $1/\rho$ we should get a straight line intercepting the G_e axis at G_d . Fig. 3.14 is such a plot for both K(Rb) and K samples. Note that G_d for the K(Rb) and K samples has the same value within the experimental error: $G_d(K(Rb)) = -1.78 \pm 0.19$ (1/V) and $G_d(K) = -1.97 \pm 0.02$ (1/V). This means that G_d is independent of the type of impurity which is present in the sample. For K(Rb) the dominant impurity is Rb, and for our pure K sample we have unknown impurities with vacancies present in samples K2-K5. Note samples K-6 and K-7 have

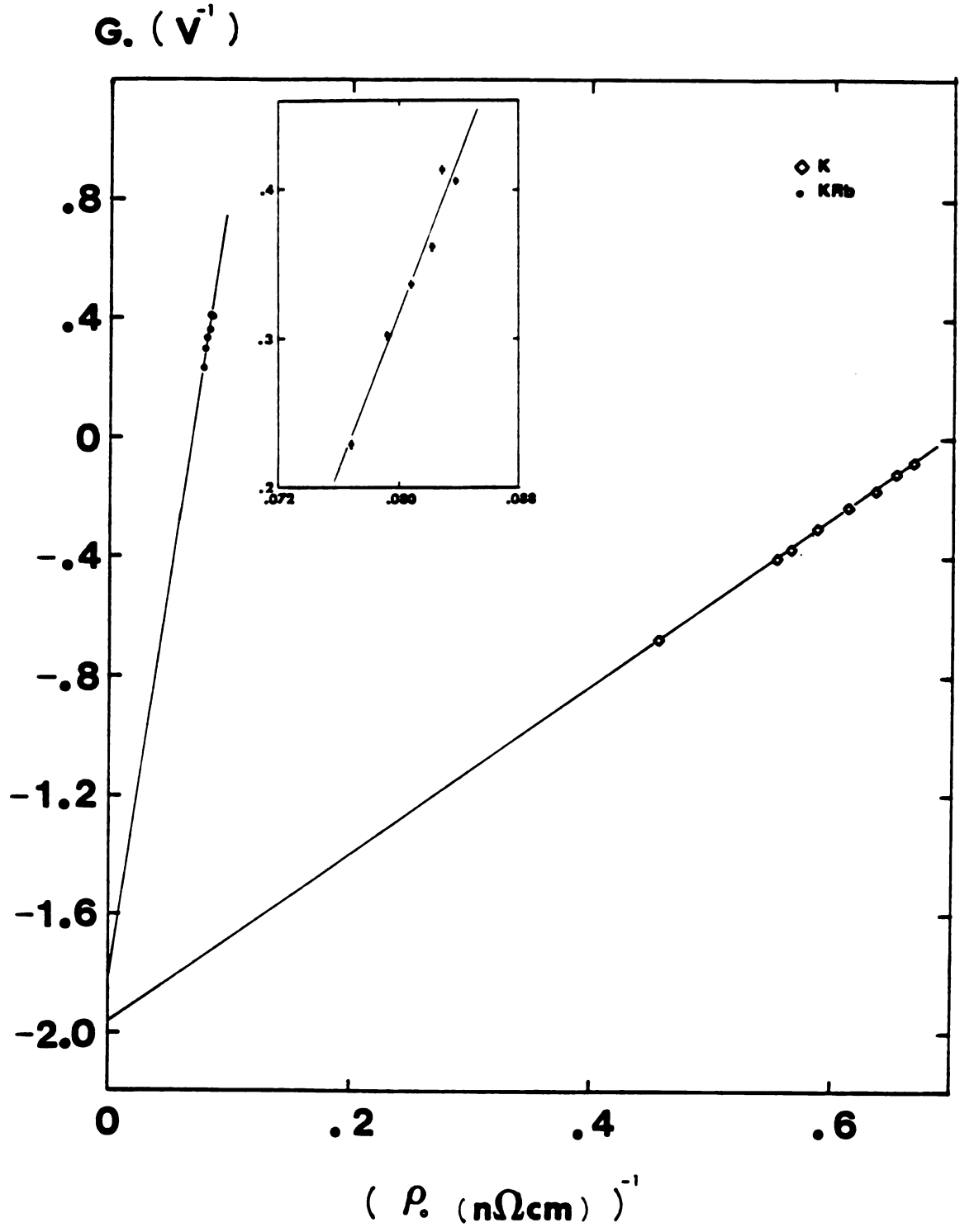

Figure 3.14
A Gorter-Nordheim plot for both K(Rb) and K samples
G_d seems to be the same in both cases.

vacancies being annealed out, and yet their G_o's also follow the same straight line as K-2 to K-5. The simplest interpretation of this unusual result is that G_o for vacancies is very similar to G_d.

Fig. 3.15 is the plot of the coefficient b of the phonon drag term vs $\Delta\rho_o$ for both K(Rb) and K samples. As is expected, we see that dislocations also suppress the phonon drag term, which is consistent with our $d\rho/dT$ measurements. Note that the presence of Rb impurities also tends to suppress phonon drag.

No systematic changes have been observed for a, the coefficient of the linear term we used in G. Its value is about 0.10 (1/VK) for all samples except for K-6, K-7 and K-8 where it jumps to 0.20 (1/VK). No theory has been found to explain this term so far.

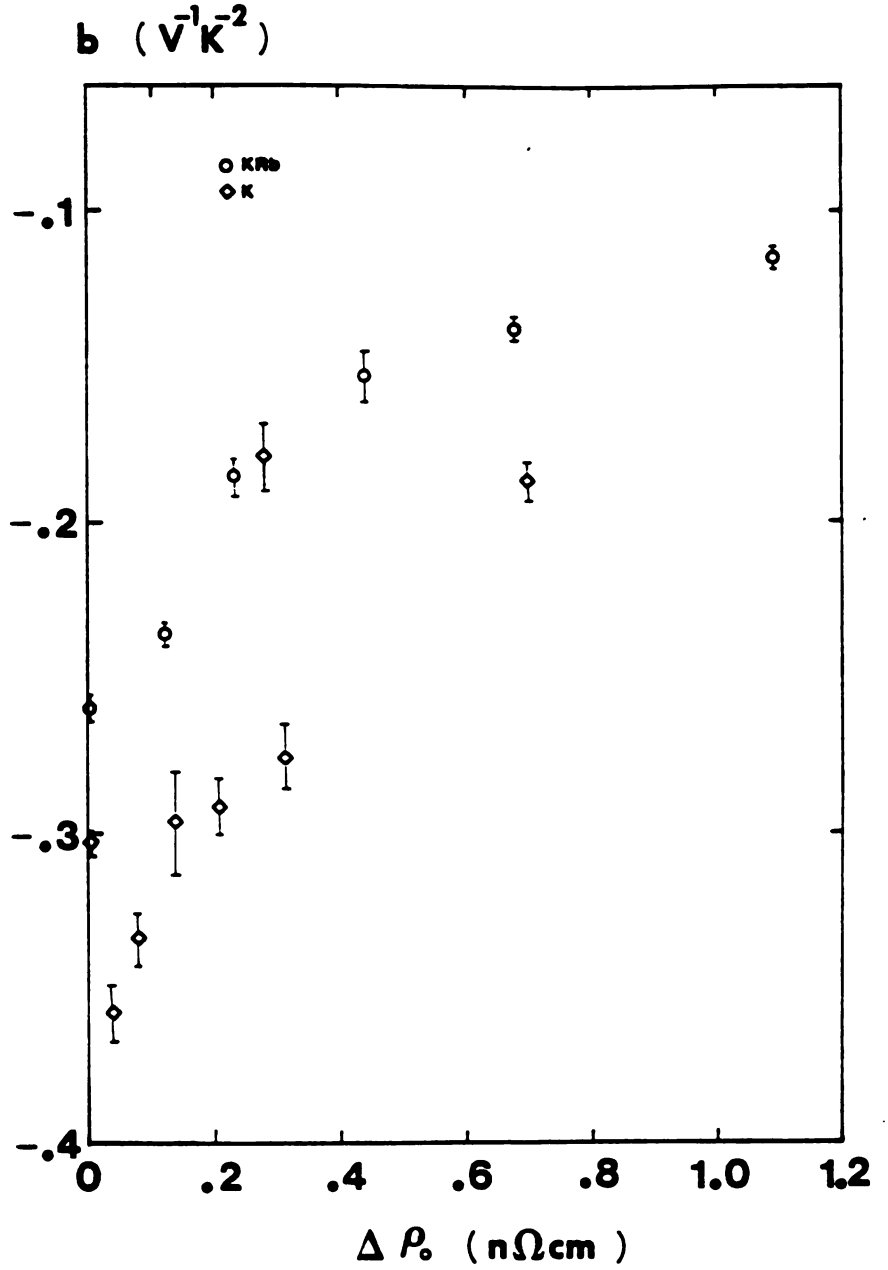

Figure 3.15
b vs $\Delta\rho_o$ for both K(Rb) and K samples
A systematic change is visible.

Chapter IV Discussion and Conclusions

Deformation has a profound influence on the electrical properties of potassium. The residual resistivity of pure K has been found to increase linearly with the twist-angle of deformation for small angles ($\theta < 1400^{\circ}$) at 9.3K. However, a tendency toward saturation in $\Delta\rho_0$ is also observed when the twist angle $\theta > 4800^{\circ}$ at 60K, and this is probably due to the high mobility of dislocations at this temperature so that close dislocations with opposite Burgers vectors are more likely to annihilate each other. For the K(Rb) samples which are deformed at 60K or the K samples which are deformed at 9.3K without annealing (where impurities or vacancies are present), the electron-dislocation interaction can be described by a vibrating dislocation model proposed by Gantmakher and Kulesco (Eq. 1.27). However, a two-frequency model has been used to give a better fit for sample KRb-4, which is twisted 4800° at 9.3K and then annealed at 35K, and sample K-5, which is twisted 1329° at 9.3K without annealing. The temperature is limited to $T < 0.6K$ where the phonon contribution is negligible. Deformation also suppresses the phonon drag which exists in the unstrained samples. The coefficient C of this Normal electron-phonon term CT^5 has been found to be ~ 0.30 $f\Omega m/K^5$, which is less than its maximum value 0.35 $f\Omega m/K^5$ predicted by Fröbose (56).

The coefficient of the vibrating dislocation term D increases

close to linearly with the change in ρ_o due to deformation. This is expected because D should be proportional to the total dislocation length in the sample. D vs $\Delta\rho_o$ for K(Rb) samples apparently has a much higher slope (Fig. 3.7) than the pure K samples. However, we know the increase in ρ_o for K when it is deformed at 9.3K contains also the contribution of vacancies which could be as large as 70% of the total increase in $\Delta\rho_o$. If the vacancy contribution is corrected for, this slope for the K samples increases and becomes about 67% of the slope for K(Rb). The remaining discrepancy in the slopes might be ascribed to the higher yield stress in potassium when the Rb impurities are added, since it is observed that K(Rb) has a higher yield stress than pure K at room temperature by us and at liquid nitrogen temperature by Hands and Rosenberg.(59)

The characteristic energy E of this vibrating dislocation term seems to have a $\Delta\rho_o$ dependence for the K(Rb) sample (Fig.3.8). For the K sample this dependence appears to be smaller. However, if we correct $\Delta\rho_o$ for the vacancy contribution to the pure K sample in the same manner as in Fig.3.7, then the slopes in Fig. 3.8 could be the same for both samples, with K(Rb) having on average a larger E. If we use the Granato elastic band model of the vibrating dislocations, we might be able to explain the $\Delta\rho_o$ dependence in E, since the frequency is proportional to the square root of the dislocation density. However, both slopes do not extrapolate to E=0 as $\Delta\rho_o \to 0$, and this might suggest some other mechanisms.

The average Rb-Rb atom distance in our alloy is about 50Å. If we

use the Tsivinskii model (Eq.1.10) with an ion radius for K of $x = 1.33\text{Å}$ and $x_o = 0$ for the case of vacancy, we can obtain the average vacancy-vacancy distance for the most severly deformed sample K-5 ($\rho_v = 0.5\ n\Omega cm$) to be about 240Å. If we use Eq.(1.8), the corresponding dislocation separation is about 4000Å ($\rho_d = 0.2\ n\Omega cm$ for K-5). If we think that the dislocation is a pinned elastic band of length 4000Å, its resonant vibrating frequency is about 1.5×10^9 Hz or the characteristic energy E is about 0.1K for sample K-5, which is a reasonable value if we compare it with the experimental value for K-5: $E \cong 0.2K$. The K(Rb) apparently has a higher value for E than that of the K sample, even if the vacancy contribution is corrected for in the pure K samples. This might be ascribed to the presence of the Rb impurity which modifies partially the pinning distances of the oscillators so that the average pinning distance becomes smaller, and thus the characteristic energy E is higher. If we use the Rb or vacancy separation length as the pinning length, then we would obtain an E with a value much higher than our experimental ones. If we use the model (Eq.1.26) in which the dislocations oscillate within the Peierls potential, we might not expect any $\Delta\rho_o$ dependence in E. However, this is not always true: if the yield stress σ_p depends on the concentration of either impurities or dislocations, we might have a $\Delta\rho_o$ dependence in E. We are planning to explore further the impurity dependence of E and D by deforming K(Rb) alloys with different Rb concentrations. We also want to see if there exists a vacancy contribution to E or D for K(Rb) samples, since our K(Rb) samples were

all annealed above 35K where most vacancies were annealed out. Thus we plan to deform K(Rb) alloys at 9.3K and measure $d\rho/dT$ below 1K.

For our 60K annealed pure K samples where the vacancies are annealed out, we see a peak in $d\rho/dT$ which cannot be fit by the vibrating dislocation model, even with a two-frequency one. It is found that this peak does not depend on the process of annealing, since our sample K2-2, which was directly deformed at 60K, also shows the peak in $d\rho/dT$. This peak is apparently suppressed by the impurities because we do not see any of this in the K(Rb) samples which were also annealed at 60K. By letting A vary we can get an improved fit even with the one-frequency vibrating dislocation model. However, the drop in A is hard to explain considering that the theory of Kaveh and Wiser(19) predicts an increase in A after deformation. The drop in A might be associated with the rearrangement of the Q-domain structure predicted by Bishop and Lawrence(4), but a more detailed theory is needed before this idea can be explored experimentally. This unusual peak can be fit instead by keeping A fixed and by adding a new term to the vibrating dislocation model, and this new term is the localized-energy-level model associated with dislocations which was proposed also by Gantmakher and Kulesco in the same paper.(33) An alternative term from Fulde and Peschel (Eq.1.24) was actually used to obtain the same fit because it gave more sensible values for the fitting parameters.

The appearance of this localized-energy-level term raises the possibility that annealing the K sample at 60K porduces a rearrangement of this energy-level distribution and that the energy-level

distribution before annealing produces a behavior in $d\rho/dT$ which looks like the vibrating dislocation model. This idea also needs to be further explored.

For our G data we obtain reasonably good fits by using Eq. (1.40) for our unstrained samples. However, a new peak is visible for the strained K(Rb) and K samples. An empirical term, aT, which has no theoretical explanation, has been added to obtain the best fit. The Gorter-Nordheim plot (Fig.3.14) exhibits good straight-line behaviors for both the K(Rb) and K samples. The characteristic diffusion term G_d due to dislocation scattering is found to be the same for both samples. Analysis of this Gorter-Nordheim plot for pure K suggests that the dislocation scattering and vacancy scattering produce quite similar contribution to G_0. If this is not the case, then the Gugan and Gurney assertion that vacancies anneal out above about 10K must be re-examined. For example, the above behavior for the G_0 of pure K could be explained as being due to lowering of the dislocation density rather than a reduction of vacancy density as the sample is warmed from 9K to 60K.

This study has been a continuation of M. Haerle's work, with emphasis on the electron-dislocation interaction in K below 1K. By using a completely different mechanism of deformation with much better control of sample geometry, we have observed similar behaviors in $d\rho/dT$. By using a second dilution refrigerator, we extended the lowest temperature down to 20 mK, which is much lower than that of Haerle's (80mK). This extended region has helped us in determining the

multi-frequency spectrum of the vibrating dislocations. We used 2mm diameter samples to avoid the complication of the size effect observed in Haerle's work.

LIST OF REFERENCES

LIST OF REFERENCES

1) I.M. Templeton, J.Phys, F: Met. Phys, 12, L121(1982)

2) T.M. Giebultowicz and et al., Phys. Rev. Lett. 56, 1485(1986)

3) H. You et al., The Proceeding of APS March Meeting 32, No.3, 445(1987)

4) Bishop and Lawrance, Phys. Rev. B 32, 7009(1985)

5) M.L. Harele et al, J.Phys. F: Met. Phys. 13, L243(1983)

6) M.L. Haerle et al., J.Low Temp. Phys.,62,Nos. 5/6, 397(1986)

7) Tsivinskii, Phys. Stat. Sol.(a) 80, 439(1983)

8) Z.S. Basinski, J.S. Dugdale and A. Howie, Philos. Mag.8,1989(1963)

9) R.A. Brown, Can. J.Phys.60,766(1982)

10) Gurney and Gugan, Phil.Mag.,24,857(1971)

11) D. Gugan, Philos. Mag. 31, 453(1975)

12) F. Bloch.,Z.Phys. 59,208(1930)

13) D. Gugan, Proc.R.Soc. Lond. A. 325,223(1971)

14) J.W. Ekin and B.W. Maxfield, Phys.Rev. B 4, 4215(1972)

15) H. van Kempen et al., J.Phys.F: Met.Phys 11,597(1981)

16) Danino, Kaveh and Wiser, J.Phys. F: Met.Phys.13,1665(1983)

17) Kaveh and Wiser, Phys.Rev.B 9,4042(1974)

18) R. Taylor et al., J. de Phys. 39,C6-1058-59(1978)

19) Danino, Kaveh and Wiser, J.Phys. F: Met.Phys. 12,L256(1982)

20) Hans-Lennard Engquist,Phys. Rev. B 25, 2175(1982)

21) J.M. Ziman, Electrons and Phonons, Oxford Univ. Press, London,1960

22) van Kempen et al., Phys. Rev.Lett. 37, 1574(1976)

23) Levy et al., Phys. Rev.Lett. 43, 1822(1979)

24) J.A. Rowlands et al., Phys. Rev.Lett.40,1201(1978)

25) M.F.Bishop and A.W.Overhauser, Phys.Rev.B. 23, 3638(1981)

26) C.W. Lee,W.P.Pratt Jr.,J.A. Rowlands and P.A. Schroeder, Phys.Rev.Lett.45,1708(1980)

27) Z.Z.Yu et al., Phys.Rev.Lett.52,368(1984)

28) R.N.Gurzhi, Sov.Phys. JETP 17,521(1963)

29) W.E.Lawrence and J.W. Wilkins,Phys.Rev.B. 7,2317(1973)

30) A.H.MacDonald et al., Phys.Rev.B 23,2718(1981)

31) Kaveh and Wiser, J.Phys.,F:Met.Phys. 10,L37(1980), 12, 935(1982)

32) H.J. Fockel, Phys. Stat. Sol. (b) 139, 59(1987)

33) Gantmakher and Kulesco, Sov.Phys. JETP 40, No.6, 1158(1975)

34) P. Fulde and I. Peschel, Adv. Phys. 21, 1(1972)

35) S.G. O'Hara and A.C. Anderson, Phys.Rev.B. 10,574(1974)

36) S.G. O'Hara and A.C. Anderson, Phys.Rev.B. 9,3730(1974)

37) A. Granato, Phys.Rev.111, NO.3, 740(1958)

38) Z.S.Basinski et al, Acta Met. 29, 801(1981)

39) Z.S.Basinski, private communication

40) A.W. Overhauser, Adv. Phys. 27, No.3,343(1978)

41) M.F. Bishop and A.W. Overhauser, Phys.Rev.B. 23, 3638(1981)

42) C.W. Lee et al., Phys.Rev.B 25, 1411-14(1982)

43) J.E. Black, Phys.Rev.B 21, 3279(1980)

44) L. Nordheim and C.J. Gorter, Physica 2,383(1935)

45) F.J.Blatt, P.A. Schroeder, C.L. Foiles and D.Greig, Thermoelectric Power of Metals, Plenum Press(1976)

46) A.M. Guenault and D.K.C. MacDonald, Proc. R. Soc. A. 274 154(1963)

47) M. Haerle, Ph.D. thesis, Michigan State Univ., p.34(1983)

48) J. Imes, Ph.D. Thesis, Michigan State Univ. (1974)

49) J. Imes, G. Nieheisel and W. Pratt Jr., J. Low Temp. Phys. 21, 1(1975)

50) V.O. Heinen, Ph.D. Thesis, Michigan State Univ., (1983)

51) O. Lounasmaa, Experimental Principles and Methods Below 1K, Academic Press, Inc. New York(1974)

52) D. Edmunds, W. Pratt Jr. and J.A. Rowlands, Rev. Sci. Inst. 51, 1516(1980)

53) G.I.Kulesco and T.B.Borzenco, Sov. Phys. Sol. St. 22, 443(1980)

54) R.J.M. van Vucht: Low Temperature Transport Properties of Simple Metals, Thesis, Univ. of Nijmegen(1984)

55) J.Bass, M.L.Haerle, W.P.Pratt Jr.,Y.J.Qian,P.A.Schroeder, S.Yin, Z.Z. Yu, and J. Zhao, Phys. Rev. Lett. 56, 957(1986)

56) K. Frobose, Z.Phys. B 26, 19(1977)

57) B.A. Hands and H.M. Rosenberg, The Low Temp. Yielding and Flow of K and Its Alloys, Acta Met. 17, 458(1969)

58) A.H. Cottrell, The Mechanical Properties of Matter, Wiley, N.Y. 1964 p.124

59) B.A. Hands and H.M. Rosenberg, Acta Met., Vol.17, April. 455(1969)